Journal of Geophysical Research – Atmospheres

Supporting Information for

Southern Ocean Precipitation Characteristics Observed from CloudSat and Ground Instrumentation during the Macquarie Island Cloud & Radiation Experiment (MICRE): April 2016 to March 2017

Emily Tansey[1], Roger Marchand[1], Alain Protat[2,5], Simon P. Alexander[3,5], Saisai Ding[4]

[1]University of Washington

[2]Australian Bureau of Meteorology, Melbourne, Australia

[3]Australian Antarctic Division, Hobart, Australia

[4]Ocean University of China

[5]Australian Antarctic Partnership Program, Institute for Marine and Antarctic Studies, University of Tasmania, Hobart, Australia

Contents of this file

Introduction

Section S1 of this document details the Parsivel Improved Rates and Types (PIRAT) algorithm. Section S2 details the blending algorithm, featuring subroutines to combine the radar, Parsivel disdrometer and tipping bucket. Section S3 provides additional figures and material pertaining to CloudSat analysis, including longitudinal and latitudinal variations in CloudSat retrievals near Macquarie Island. Section S4 provides a table of averaged seasonal and annual precipitation rates from the tipping bucket for the years 2002-2016 and CloudSat retrievals for 2006-2017. Section S5 examines the effect that CloudSat sampling has on capturing annual and seasonal variability in accumulated surface precipitation. Section S6 compares radar Doppler and mean PIRAT particle velocities. Lastly, Section S7 shows the results of the bootstrap resampling significance test of the diurnal cycle.

S1. Parsivel Improved Rate and Types (PIRAT) algorithm

This document describes the PIRAT algorithm subroutines. The purpose of this algorithm is to determine the particle type (rain, snow, ice, wet snow) from Parsivel measurements when particles are large enough to have appreciably different fall velocities for each precipitation type. This information is subsequently used in the estimation of precipitation rate, effective radius and particle size distributions (PSDs) for the Parsivel. The algorithm contains procedures that attempt to correct for problems with margin fallers and wind-induced splashing errors, among other factors. Data output by the Parsivel vendor's proprietary algorithm, specifically histograms of particle counts by size and velocity commonly referred to as the size-velocity spectra, serve as the primary raw input. The PIRAT algorithm can be accessed at *https://github.com/etansey/PIRAT_algorithm*.

The PIRAT algorithm output is later blended with tipping bucket and radar retrievals to create a combined best estimate for near surface precipitation. This blending algorithm is described in Section 2.

The overall flow of the PIRAT algorithm is shown below in Figure S1.

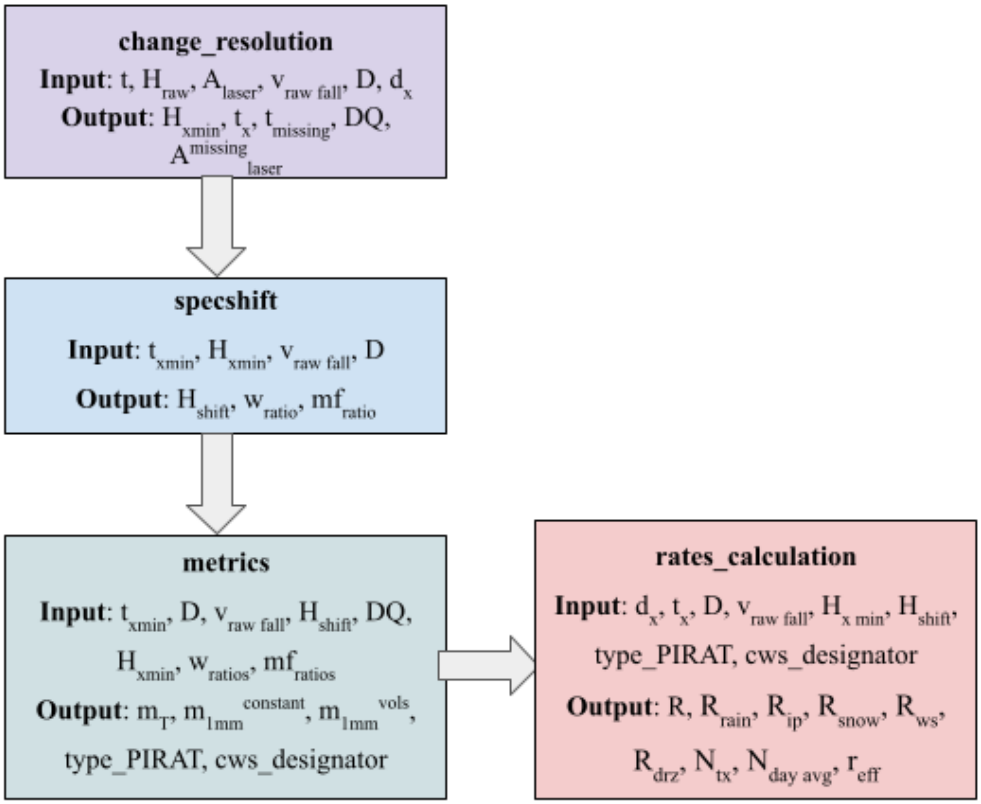

Figure S1: PIRAT flow chart.

S1.1 change_resolution(t, H_{raw}, A_{laser}, $v_{raw\ fall}$, D, d_x)

The first step in the algorithm is to reduce the resolution from the vendor's 1-minute data to a user-defined scale. We found that reducing the time resolution to 5 minutes significantly increases counts for larger particles that are critical to obtain a reasonable particle type classification. The 'change_resolution' subroutine first identifies any missing timesteps (1-minute samples in the raw data) and creates a 1-minute resolution daily array (length=1440) with NaN values assigned to any 1-minute periods in which there are missing data. This NaN-filled data is then used to create a reduced resolution version of the size-velocity spectrum, summing histogram counts over a fixed number of 1-minute timesteps, specified by the integer d_x.

This subroutine also initiates a Data Quality (DQ) flag integer array. The bits in the DQ flag indicate the presence of missing data, or in later processing, when the data have been "renormalized". As detailed later in the 'rates_calculation' section, "renormalization" is a bulk correction applied when the data is of low quality (and such data are not used in the analysis in the main text).

The inputs for this subroutine include the raw timestamps and raw laser power amplitude arrays, and the size-velocity spectra. Specifically:

- H_{raw} – Parsivel's observed particle size-velocity histogram
  - dimensions: (t, $v_{raw\ fall}$, D); unit: counts
- t = 1-minute time array; unit: seconds
- $v_{raw\ fall}$ = array of raw fall velocity for spectrum bins (32 bins, unit: m/s)
- D = array of effective particle diameters for spectrum bins (32 bins, unit: mm)
- A_{laser} – 'laser_amplitude'
  - dimension: t; unit: arbitrary counts
- d_x – 'divisorx' – PIRAT user-defined integer divisor, to decrease 1-minute spectral resolution to e.g. 5-minute resolution

Output returned by 'change_resolution':

- H_{xmin} – 'rawspecxmin' – using H_{raw}, x-minute resolution size-velocity spectra are created. Note: for this work, x=5.
  - dimensions: (t_x, $v_{raw\ fall}$, D); units: counts
- t_x = x-minute timesteps (e.g. 288 for 5-min res.)
  - dimension: t/d_x; units: seconds
- $t_{missing}$ = Parsivel's 'time' array with filled in values in places where the instrument cut out
  - dimension: $t_{missing}$; units: seconds
- DQ = data quality flag array
  - dimension: t_x
  - bit 1 = 'missing all spectra' means all spectra (x-min resolution) are missing due to instrument issues; histogram of zeros is added to pad missing time
  - bit 2 = 'missing at least 1 spectrum out of x minutes' means out of x minutes, some number (one or more) of measurements are missing and this bit will be turned on

- bit 3 = ‘renormalized’ before calculations (PSD, effective diameter, rate). Counts from noise regions are added to median bins (this bit is turned on in the subroutine ‘rates_calculation’, as needed).

- $A^{missing}_{laser} = A_{laser}$ with NANs in places where the instrument cut out
  - dimension: $t_{missing}$

S1.2 specshift(t_{xmin}, H_{xmin}, $v_{raw\ fall}$, D)

Strong horizontal winds or near-surface turbulent gusts result in the Parsivel underestimating the fall velocity of particles and greatly increases the occurrence of margin fallers and “wind-induced” counts (each of these described below), and generally create some “spectral blurring,” visible in Fig. S3a. We observed that the mean fall speed with size relationships were too low during nearly all MICRE rain events observed and required some velocity correction. This subroutine removes noise and applies an upward velocity shift *dv* to counts in bins of the particle size-velocity histograms, as demonstrated in Fig. S3. Again we found 5-min resolution was important to accomplish this. Details of the *dv* calculation are given below (A1.2.2). Before applying this shift, the ‘specshift’ algorithm first identifies which spectra are candidates for velocity shifting by considering the number of counts in the margin faller and windy noise regions of a spectrum (Fig. S2a). The algorithm (schematic shown in Fig. S4) takes the following into account:

(i) large (likely frozen or partially frozen) particles falling at reasonable speeds → no shift applied, as spectrum is likely frozen precipitation

(ii) high counts (20 or more) in the histogram bins corresponding to snow → no shift applied, as spectrum is likely frozen precipitation

(iii) **a.** counts show up in the margin fallers region (>0.1% of whole spectrum's counts) **b.** either >3 counts in wind noise region, or **c.** <20 counts in snow region **a. + b.** or **a. + c.** → shift applied, as spectrum is likely liquid precipitation.

S1.2.1 Margin faller and wind-induced noise

Margin fallers are particles that don't pass through the full laser beam cross section but pass through the sides of the beam. As a result, they appear as small particles with high velocity since they block only a small portion of the broadened laser beam and are only observed for a very short period. These unphysical margin faller counts (region shown in Fig. S2) are removed for later processing. We observed that margin fallers are much more prevalent during periods with certain liquid (rather than frozen) precipitation, suggesting that splashing against the Parsivel detector covers likely increases their presence.

Similarly, large and slow moving particles appear in Parsivel size-velocity spectra during rainy and windy conditions (region labeled windy in Fig. S2) and are presumably newly formed particles arising from splashing or dripping where the newly-generated particles have not accelerated to terminal velocity (nor had a chance to break apart as a result of drag). These counts are also removed from later processing, but likewise are indicative of liquid precipitation being present.

(a)

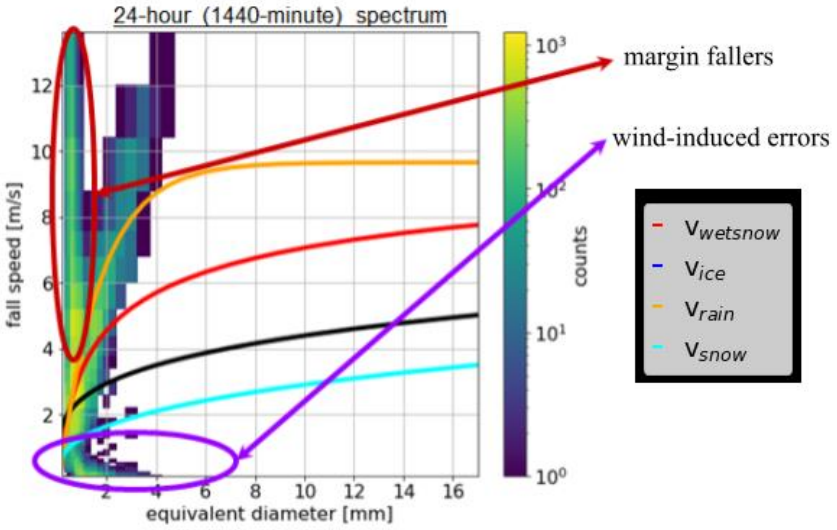

126

(b)

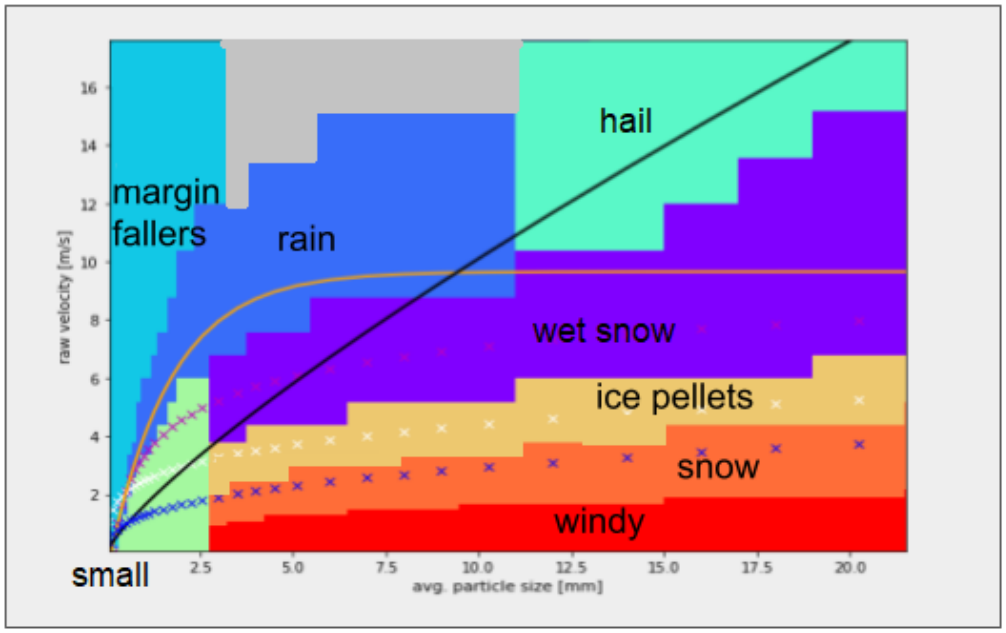

127

128 *Figure S2:* ***(a)*** *Full day raw histogram as measured by the Parsivel on a day with only warm*
129 *drizzle and rain events. Non-noise counts fall below the rain terminal fall curve* $v_{rain} = v_{GK}$*,*
130 *indicating that a shift is necessary.* ***(b)*** *Defined regions of the histogram spectrum referenced in*
131 *'shiftspec' subroutine.*

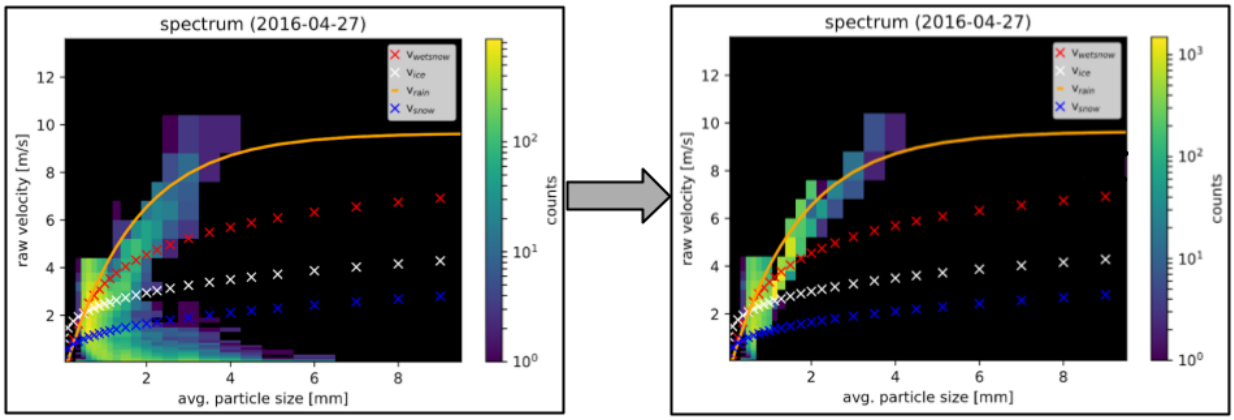

Figure S3: An example of a rain spectrum under windy conditions (left) and the same spectrum after application of the wind shift factor dv.

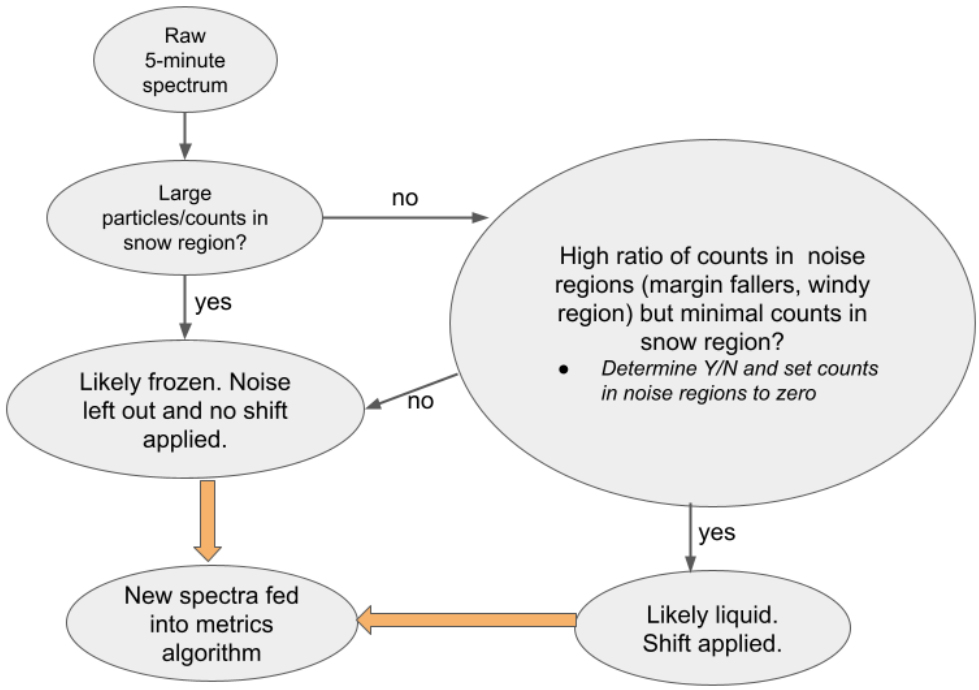

Figure S4: Schematic of 'shiftspec' subroutine.

S1.2.2 Upward shift *dv* for precipitation falling too slowly

A variety of size-to-fall-velocity relationships for rain drops have been developed over the years. Fig. S2 (gold curve) shows the widely used relationship of Gunn & Kinzer [1949], given by

$$v_{GK} = 9.65 - 10.3 \times e^{-0.6D}$$

where v_{GK} is the raindrop terminal fall speed with units m/s, and D is the particle diameter. We found that peaks in the Parsivel size-velocity spectra frequency fell below this expected relationship. The difference between the expected curve and the peak in the measured size

spectra for precipitation events associated with warm clouds were used to develop a velocity correction. Based on discussions of this effect in existing literature, e.g. Friedrich et al. [2013], we thought that the error might be correlated with wind speed (measured at the Macquarie Island station), the component of wind along the laser beam (north in our case) or the number of counts in the windy or margin faller regions of the spectra. But we found no significant correlation with any of these variables (see for example Fig. S5), only that a certain number of margin fallers or wind-counts was indicative of the presence of an offset. The north component of the wind velocity was typically larger than 10 m/s when this occurred.

The error, however, is a strong function of the drop diameter. The average difference between *observed* fall velocity (v_{obs}) and v_{GK} was composited for 5 months of warm rain data and fit to a polynomial to generate a correction curve (shown in Fig. A6):

$$dv = p_0 + p_1 \times D + p_2 \times D^2 + p_3 \times D^3$$

$$[p_3, p_2, p_1, p_0] = [-0.157, 1.255, -1.968, 2.905]$$

Input for 'specshift':

- $H_{x\ min}$
- t_x
- $v_{raw\ fall}$
- D

Output returned by 'specshift':

- H_{shift} = 'shiftspec' shifted velocity-size histogram spectrum
  - dimension: (t_x, $v_{raw\ fall}$, D); unit: counts
- w_{ratio}, mf_{ratio} – ratios of counts in wind and margin faller noise regions to total counts in spectrum
  - dimension: t_x

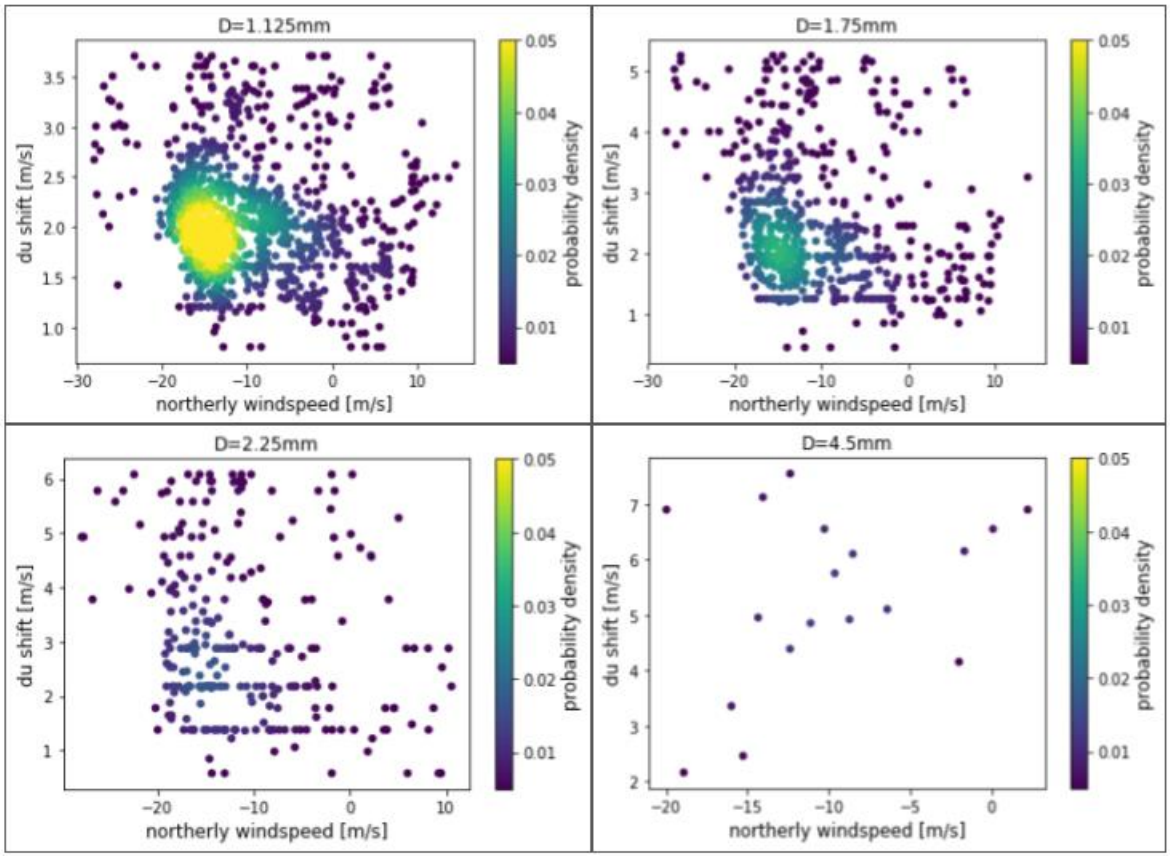

Figure S5: Necessary upward shift on velocity axis ($dv = v_{GK} - v_{obs}$) vs. northerly wind speed as measured at the Macquarie Island station. The color bar shows normalized probability density. The scatterplot mean regions (yellow dots) occur at higher dv values as diameter increases. Uses MICRE data from April-August 2016 warm rain events.

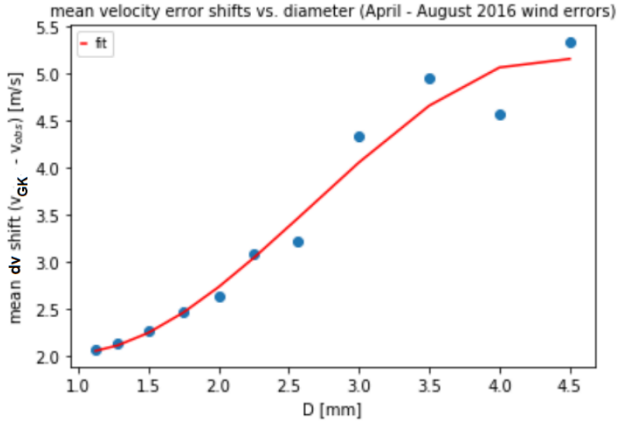

Figure S6: Polynomial curve fit for dv as a function of effective diameter. Blue points correspond to the probability density means (yellow centers) in Fig. S5. Uses MICRE data from April-August 2016 warm rain events.

S1.3 metrics(t_{xmin}, D, $v_{raw\ fall}$, H_{shift}, DQ, H_{xmin}, w_{ratios}, mf_{ratios})

This subroutine classifies the phase of precipitation by considering the most populated bins in H_{shift}.

If the distribution is not dominated by small particles (discussed below), a metric – m_T, given below – is used to identify the type. Here, the subscript T represents the precipitation 'type' which can be rain, wet snow (equivalently, mixed phase particles), ice pellets and snow. The type with the largest value for m_T is identified as the most likely precipitation type.

$$m_T = \left(\sum_{i=9}^{32} \sum_{j=1}^{32} C_{i,j} \times \left(\frac{v_{\sigma T}(i)}{v_{\sigma T}(i) + \Delta v_T(i,j)} \right)^k \right) \div \sum_{i=9}^{32} C_i$$

Subscripts i, j refer to the i^{th} diameter and j^{th} velocity bin, with i ranging from 9 (above 1 mm) to 32, j from 1 to 32; $C_{i,j}$ are the counts in one individual bin, C_i is the counts in the i^{th} diameter column; $v_{\sigma T}(i)$ is the standard deviation of the spectrum used to calculate v_{fit} for each type. With the exception of rain, v_{fit} are the empirical fall speeds found by curve fitting various spectra as described below. $\Delta v_T(i,j) = |v_{obs}(j) - v_{fit}(i)|$, the difference between an occupied velocity bin and v_{fit}; k = 3 was subjectively chosen by trial and error. Only diameters larger than 1 mm (i^{th} bin 9) are used to calculate m_T.

As mentioned previously, the rain terminal fall speed equation is taken from Gunn & Kinzer [1949]. Empirical fall speeds for ice pellets and snow were calculated using the Parsivel vendor's designation of particle phase, called "weather codes". Simply, if a sufficiently large fraction of counts occurred in the region labeled "ice", then the spectrum is identified as containing ice.

We took spectra from April-June 2016 identified as snow and ice pellets according to the vendor's weather codes. Power law equations ($v_{fit} = aD^b$) were fit to the data and standard deviations $v_{\sigma T}$ taken across all events in each category were calculated. The resulting coefficients are:

$$[a_{ip}, b_{ip}] = [2.476, 0.250] \text{ for ice pellets,}$$

$$[a_s, b_s] = [1.291, 0.353] \text{ for snow.}$$

The resulting v_{fit} for v_{ip} and v_{snow} match the range of parameters reported by other studies for power law fall speed functions of diameter and velocity magnitudes [Magono & Nakamura, 1964; Locatelli & Hobbs, 1974]. The rain, ice pellets and snow regions were defined using the empirical fall speed equations, plus one standard deviation of bins surrounding these plotted curves as shaded in Fig. S2b. The wet snow region was taken as the space between the ice pellet and rain regions, and the wet snow curve was defined by keeping counts in the wet snow region pictured in Fig. S2b from all spectra April-June, and then calculating a wet snow fall speed relationship for the wet snow region. The metric calculation is not explicitly limited to counts in these regions. Wet snow was found to fit the curve $v_{ws} = k_{ws} - a_{ws} * \exp(-D^{bws})$ better than a power law, where a_{ws} = -13.919, b_{ws} = -0.344 and k_{ws} = -1.783 m/s.

Some additional filtering is also done to eliminate occasional outlier events. Specifically:

1) Spectra with m_r as the highest metric do not get classified as rain if there are 5 or more counts in diameter bins greater than 5 mm, the nominal maximum raindrop size. If larger particles are present and m_r is largest, the second-largest metric is used define the most likely type.
2) If subroutine 'specshift' failed to identify a spectrum that should have been velocity shifted, or if the *dv* shift was not enough, then rain spectra can be miscategorized as wet snow or ice pellets. An additional filter is included here to identify these events. Specifically, if a classification shows only one wet snow/ice pellet class in a 30-minute period that is otherwise surrounded by rain and small classes, and $m_{wet\ snow/ice} - m_{rain} < 0.15$ (meaning a marginal classification), the class is changed from wet snow/ice pellet to rain.
3) During instrument calibration periods, the instrument pulses the laser beam and creates a spectrum with randomly distributed counts. These periods are also identified and flagged in this subroutine.

5-minute spectra are categorized as 'small' if the following metric is larger in comparison to m_T for rain, ice pellets, wet snow or snow:

$$v_{small} = 1 - \frac{\#\ large\ bin\ counts}{7}$$

The threshold of 7 counts was chosen by inspection of 200 spectra (5-minute size-velocity spectra already processed by the Specshift subroutine). 7 counts is the minimum number of large bin counts required to determine the phase using the m_T formula.

Input for 'metrics':

- t_x
- $v_{raw\ fall}$, D
- H_{shift}, $H_{x\ min}$
- w_{ratios}, mf_{ratios}
- DQ

Output returned by 'metrics':

- m_T = metrics for rain, wet snow, ice pellets and snow
  - dimension: t_x
- m_{small} = metric for small particle precipitation
  - dimension: t_x
- 'type_PIRAT' phase classifications of H_{shift}
  - dimension: t_x
  - values are as follows: 0 = no precip, 1 = rain, 2 = ice, 3 = snow, 4 = wet snow, 5 = small
- 'cws_designator,' designates which density correction should be used for wet snow classes in 'rates_calculation' subroutine. See equations in the next section for a quantitative definition.

- dimension: t_x
  1. Compare $|m_{ip} - m_{ws}|$ and $|m_r - m_{ws}|$.
  2. If m_{ws} is more similar to m_{ip}, use a less dense coefficient in rates calculation. If m_{ws} is more similar to m_r, use a denser coefficient.
- DQ

S1.4 rates_calculation(d_x, t_x, D, $v_{raw\ fall}$, $H_{x\ min}$, H_{shift}, type_PIRAT, cws_designator)

This subroutine calculates and outputs the precipitation rate for each phase of precipitation, regardless of class assigned by 'metrics' as the most likely type. Some filtering is done based on statistics of that day's precipitation in order to decrease unrealistically high values. The PSD, effective radius and precipitation rate corresponding to each H_{shift} are also calculated as follows:

Number concentration and PSD

The laserbeam sampling cross section is defined by length L = 0.180 m and width B = 0.03 m. The Parsivel sampling area is then

$$S = L \times \left(B - \frac{\overline{D_i} \times 10^{-3}}{2} \right)$$

where $\bar{D}_i$ [unit: mm] is the midpoint of the i^{th} diameter class. Concentration of drops are calculated using this sampling area following Jaffrain & Berne [2010], with the PSD (# per m^{-3} mm^{-1}) for the i^{th} diameter given by,

$$N_i = \frac{1}{S \cdot dD_i \cdot dt} \times \sum_{j=1}^{32} \frac{C_j}{\overline{v_{fall}^j}}$$

where dD_i [unit: mm] is the spacing of the i^{th} diameter class/bin. C_j are counts in the j^{th} velocity bin and $\overline{v}_{fall}^j$ [unit: m/s] is its midpoint. Sampling time is dt = d_x × 60 seconds, or 300 seconds when using a 5 minute timescale.

Hydrometeor effective radius

The effective radius for the x^{th} spectrum of the day (r_{eff}^x) is found using the PSD third moment divided by the second moment.

$$r_{eff}^x = \frac{1}{2} \times \frac{\sum_{i=1}^{32} N_i \times D_i^3 \times \Delta D_i}{\sum_{i=1}^{32} N_i \times D_i^2 \times \Delta D_i}$$

Precipitation rates

The general rate equation used for precipitation of phase type T is

$$R_T(D) = c_T \times 6\pi \times 10^{-4} \int_{D_{i=1}}^{D_{i=32}} N_i \times v_T^{fit}(D_i) \times D_i^3 \, dD_i$$

in [mm/hour]. The density correction coefficient c_T simplifies to 1 for rain and drizzle, whereas it decreases $R_T(D)$ for frozen and semi-frozen precipitation. The following density corrections are used:

$$c_{ip} = \frac{\rho_{liquid} - \rho_{ice}}{\rho_{liquid}}$$

where ρ_{liquid} = 0.997 g cm^{-3}, ρ_{ice} = 0.934 g cm^{-3} (ice pellets)

$$c_s(D) = \frac{\rho_{snow}(D)}{\rho_{snow}(D) + \rho_{liquid}}$$

where ρ_{snow} = 0.178D$^{-0.922}$ in g cm^{-3} (snow)

$$c_{ws}(D) = \left(\frac{v_{ws}^{fit}}{v_{snow}^{fit}}\right)^g \times c_s(D) \qquad \text{(wet snow)}$$

where g = 2 when mostly melted, g = -1/3 when mostly frozen, as specified by the c_{ws} designator from 'metrics'.

The general forms of each coefficient were set to adjust $R_T(D)$ to minimize the difference between the Parsivel accumulation compared to the tipping bucket. Densities of frozen precipitation used here fall within the ranges of diameter-dependent densities reported in [Locatelli & Hobbs, 1974], Table 1.

S1.4.1. Corrections for undercounting of small particles

Comparison with tipping bucket data made clear that the Parsivel was significantly underestimating the accumulation when the spectrum was dominated by small particles (type = 1) and the spectrum contained a large number of margin fallers or windy counts. We therefore adjusted or renormalized the spectrum if

type_PIRAT = 5 and

- mf_{ratio} or $w_{ratio} > 0.5$
- $mf_{ratio} + w_{ratio} > 0.7$

If these conditions are met, 50% of the neglected noise counts were added to the median velocity bin in each diameter column where counts existed. 50% was chosen because it gives the best agreement with the tipping bucket. The tipping bucket is susceptible to systematic wind errors of its own. In particular, errors have been found to increase for precipitation events containing smaller drops and higher wind speeds [Nešpor & Sevruk, 1999]. We note that in the blend product (Section 2), the PIRAT data for all types of precipitation are again routinely renormalized to match tipping bucket accumulations. The main effect of the bulk adjustment described here is to improve PIRAT estimates when tipping bucket data are not available.

S1.4.2. Switching Type from Small to Snow, Wet Snow, or Ice

We found that periods identified as small particle precipitation that were embedded in periods of snow, wet snow, or ice appeared to produce precipitation rates (accumulations) that were too

high relative to the tipping bucket. To address this, the particle type in a 20 minute window surrounding 'small' precipitation is examined and if found to be entirely snow, wet snow or ice, the classification is changed from small to match that of the neighboring type. If the period is some combination of snow, wet snow and/or ice, it is changed from small to the nearest previous timestep's classification. This lowers the density of the particle and reduces the estimated precipitation rate.

Input for subroutine 'rates_calculation':

- t_x, d_x
- $v_{raw\ fall}$, D
- H_{shift}, $H_{x\ min}$
- c_{ws} designator
- type_PIRAT
- mf_{ratio} & w_{ratio}

Output returned by 'rates_calculation':

- R = precipitation rate array. Elements are specific to weather type identified in type_PIRAT.
  - dimension: t_x; unit: mm/hour
- R_{rain}, R_{ip}, R_{snow}, R_{ws} = precipitation rate arrays as if all weather were rain, ice pellets, snow and wet snow, respectively.
  - dimension: t_x; unit: mm/hour
- R_{drz} = array of rates using small particle bins only, even in cases where large particles were present. Cutoff bin for a spectrum's drizzle/small particle counts is D=1 mm.
  - dimension: t_x; unit: mm/hour
- N_{tx} = PSDs for each 5-min spectrum
  - dimension: (t_x, D); unit: m^{-3} mm^{-1}
- $N_{day\ avg}$ = PSD for all precipitation that day
  - dimension: D; unit: m^{-3} mm^{-1}
- r_{eff} = array of effective radii for each 5-min spectrum
  - dimension: t_x; unit: mm

S2. MICRE blending algorithm

The blending algorithm includes three steps or subroutines, shown in Figures S8-S10. In the first step, 'PIRAT_TB_merge' (Fig. S8), the tipping bucket (TB) and PIRAT are combined. In the second step, 'radar_xmin' (Fig. S9), the radar precipitation retrieval and data quality flags are reduced onto a 5 minute grid. And in the third subroutine ('blend'), the outputs of the first two subroutines are combined to arrive at a final best estimate for the surface precipitation rain rate, effective radius and precipitation type.

S2.1 PIRAT-TB merge

The PIRAT-TB merge begins with the TB and output from the PIRAT algorithm described in Section 1. TB accumulation over 2 hours, a timeframe chosen to provide sufficient time for one

or more tips under lightly precipitating conditions, is compared to PIRAT during the same period. The main points of this algorithm are as follows:

1) Blend Data Quality (DQ) flags, seen in Fig. S11b, are set for intervals where data from either instrument is missing; if 50% or more of the data in a 2-hour period is missing, the entire 2-hour period is flagged as having bad data.
2) If PIRAT is missing for 50% or more of the 2-hour period but the TB data is fine, the rate is set to be TB accumulation divided by 2 hours; the effective radius (r_{eff}) and particle type are given a value of -1, indicating "poor quality/uncertain".
3) If the tipping bucket tips twice or more over the two hours then
    a. If the PIRAT accumulation matches the TB within 0.2 mm, then PIRAT rate, effective radius and thermodynamic phase (PIRAT type) are taken as the best-estimate blend value for the 2 hours.
    b. Otherwise the PIRAT data are rescaled (described below).
4) Else if the tipping bucket tips less than twice over the two hours then
    a. If PIRAT accumulation is < 0.4 mm, then PIRAT rate, effective radius and thermodynamic phase (PIRAT type) are taken as the best-estimate blend value for the 2 hours.
    b. Otherwise the PIRAT accumulation is too large (the TB should have tipped). The 2 hours are flagged as poor quality data by turning on bits 1 and 3 of the Blend DQ flags. (Note: the PIRAT data are still kept as a blend estimate, but these poor quality data are not used in the analysis).

Rescaling: a scaling constant "alpha" is applied to the 2 hours' worth of PIRAT size-velocity spectra (denoted H_{shift} in Section 1) to increase (or in very rare cases, decrease) the amount of precipitation while keeping the shape of the PSD the same. This is done iteratively. Alpha starts out as a best guess (0.5 × tipping bucket accumulation ÷ PIRAT accumulation) and then adjusts to minimize the difference between the PIRAT & TB accumulations until they match within 0.05 mm, or until the scaling constant surpasses 40. The minimum possible scaling constant is 0.025. The value of alpha is tracked and results presented in this paper are limited to scaling constants below 20, as values larger than this are indicative of the Parsivel not working properly. Such events are not common and are typically associated with periods where the laser amplitude is well below its nominal operational intensity, suggesting this occurs when there is condensation on the instrument lens.

Note: rescaling does not change the shape of the distribution and hence does not change the effective radius or type.

The relative difference in accumulations over 2 hours, (TB accumulation - PIRAT accumulation) ÷ TB accumulation, indicates that rescaling PIRAT reduces the mismatch between instruments substantially. Plotted as a function of binned tipping bucket accumulations (ranges shown on horizontal axis) in Fig. S7, the scaled PIRAT relative error remains between ±5% for all accumulation ranges greater than 0.2 mm (one tipping bucket tip; the minimum tipping bucket accumulation for which rescaling is performed is 0.4 mm).

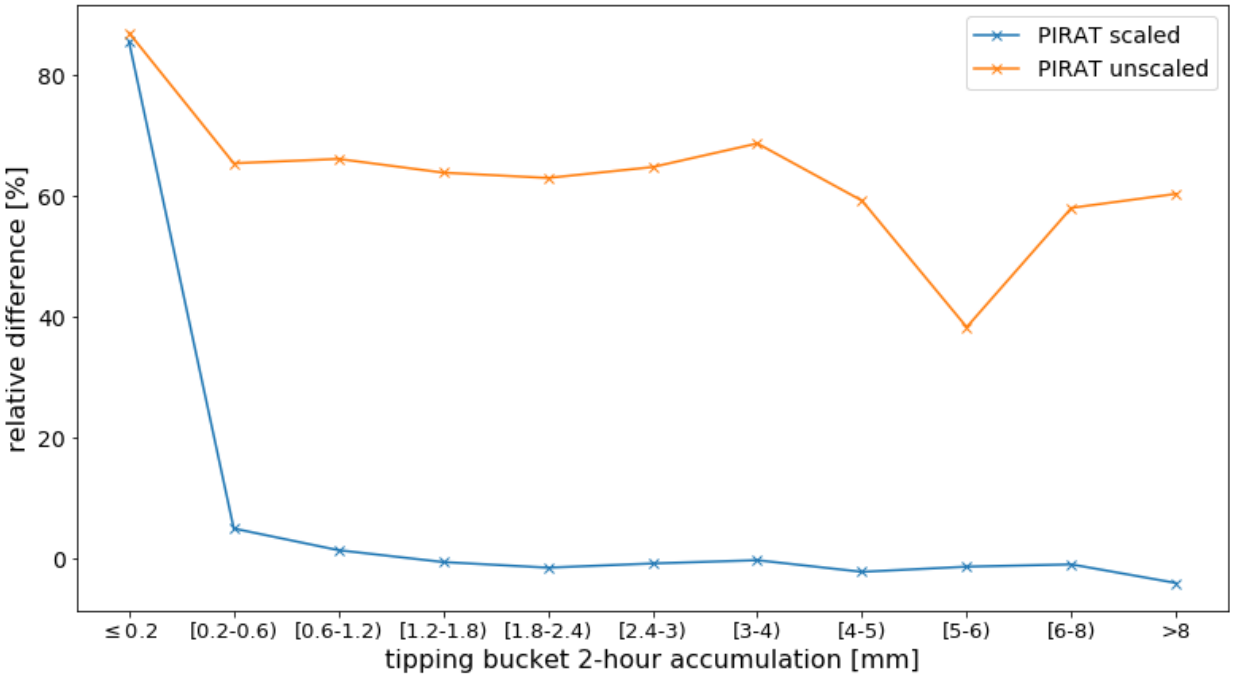

Figure S7: Relative difference in 2-hour accumulations between PIRAT and the tipping bucket for scaled (blue) and unscaled (orange) PIRAT accumulations.

S2.2 radar_xmin

"radar_xmin" reduces output from the radar reflectivity-velocity (ZV) precipitation retrieval onto a coarse (nominally 5-minute) time scale. The ZV retrieval is only intended to work for light precipitation comprised of small particles and we use here only the radar retrieval output in the range 150 to 250 m above the surface to avoid surface clutter. It assumes the reflectivity is only due to precipitation and so for reflectivity factors less than -15 dBZ, we require that cloud base from the lidar ceilometer be above 250 m; otherwise, the presence of "near surface" precipitation is considered ambiguous. The subroutine utilizes the radar precipitation (ZV) retrieval DQ flags listed in Fig. S11a. The principal outputs are:

Radar_rate: ZV near-surface precipitation rate

-1 = no retrieved rate available or rate is untrustworthy

0 = no near-surface precipitation present

>0 = the mean rate from ZV retrieval (This does not mean the rate "when present"; zeros are included in the mean if it is not raining for some subset of ZV retrievals in the 5 minute period. Subsets of any ZV retrievals without rates are excluded from the mean.)

Radar_r_{eff}: ZV near-surface effective radius

-1 = no retrieved radius available or radius is untrustworthy

0 = no near-surface precipitation is present

>0 = mean effective radius (when precipitation was present).

Radar_type: -3 = no lidar data or lidar cloud base is bad.

-2 = cloud base below 250 m and reflectivity < -15 dBZ (ambiguous precipitation)

-1 = radar data missing/bad.

0 = no precipitation is present

5 = small particle precipitation is present (but rate can still be -1 if ZV retrieval fails).

Key rules in the procedure are:

1) If 50% or more of the 5 minutes have bit 1 of the radar ZV retrieval DQ flags turned on (bad radar data), all variables are set to -1.
2) If >50% of the 5 minutes have bits 2 or 3 of the radar ZV retrieval DQ flags turned on (lidar data missing or cloud base below 250m),
    a. reflectivity between 150 – 250 m is examined to determine the likelihood of precipitation reaching the surface.
        i. For reflectivity < -40 dBZ, all variables are set to zero ("no precipitation").
        ii. For -40 dBZ < reflectivity < -15 dBZ, rate and r_{eff} are set to -1 ("poor quality/uncertain") while type is set to -2 ("precipitation ambiguous"), and Blend DQ bit 5 is turned on ("precipitation ambiguous).
        iii. For reflectivity > -15 dBZ, reflectivity is assumed to be dominated by precipitation; type=5 (small particle precip.) and processing continues.
3) If >50% of the time has other ZV retrieval warning flags turned on (Fig. S11a, bits 4 to 8*)*, this means that it <u>is</u> precipitating, but the ZV retrieval is of poor quality. Type=5, rate and r_{eff} are -1.
4) Otherwise, >50% of points have good data. Mean rates and r_{eff} are calculated from good points. Type=0 if there's no precipitation during all good points; otherwise, type=5.

S2.3 blend

Finally, the blending algorithm (Fig. S10) combines output from the "radar_xmin" and "PIRAT_TB_merge" procedures. Principal outputs are:

Blend_rate: Precipitation rate taken from either the radar or PIRAT-TB merge

-1 = no retrieved rate is available or is untrustworthy

0 = no precipitation is present

>0 = rate from either the radar or PIRAT-TB merge was selected per the logic sequence shown in the flow chart (Fig. S10).

Blend_r_{eff}: Effective radius

-1 = no retrieved radius is available or is untrustworthy

0 = no precipitation is present

>0 = mean effective radius (when precipitation was present).

Blend_type: -2 = no PIRAT-TB retrieval, cloud base below 250 m or its retrieval was missing, and radar retrieval ambiguous (could be cloud or light precip.)

-1 = means no type available (TB has precip., but PIRAT had no retrieval type)

0 = no precipitation is present

5 = small particle precipitation
1 = rain (large particles)
2 = ice pellets
3 = snow
4 = wet snow

Following the flow chart, the key rules are:

1) If no PIRAT-TB merge precipitation rate is available (rate < 0) but the radar shows precipitation (rate > 0), the radar variables are taken as the blend best estimate, and vice versa.

2) If both indicate precipitation with nonzero rates then

   a. If both indicate small (type = 5), the instrument with the larger rate retrieval is taken as the blend best estimate.
   b. If PIRAT-TB merge indicates large particles (merge type = 1, 2, 3 or 4), the PIRAT-TB merge data is used.
   c. If PIRAT-TB type = -1, the PIRAT-TB rate calculation came only from the TB. If the TB rate exceeds the radar rate by a factor of 2, the TB rate with no phase (type = -1) is taken for the blend estimate. Otherwise, the radar rate, r_{eff} and type=5 are selected for the blend estimate.

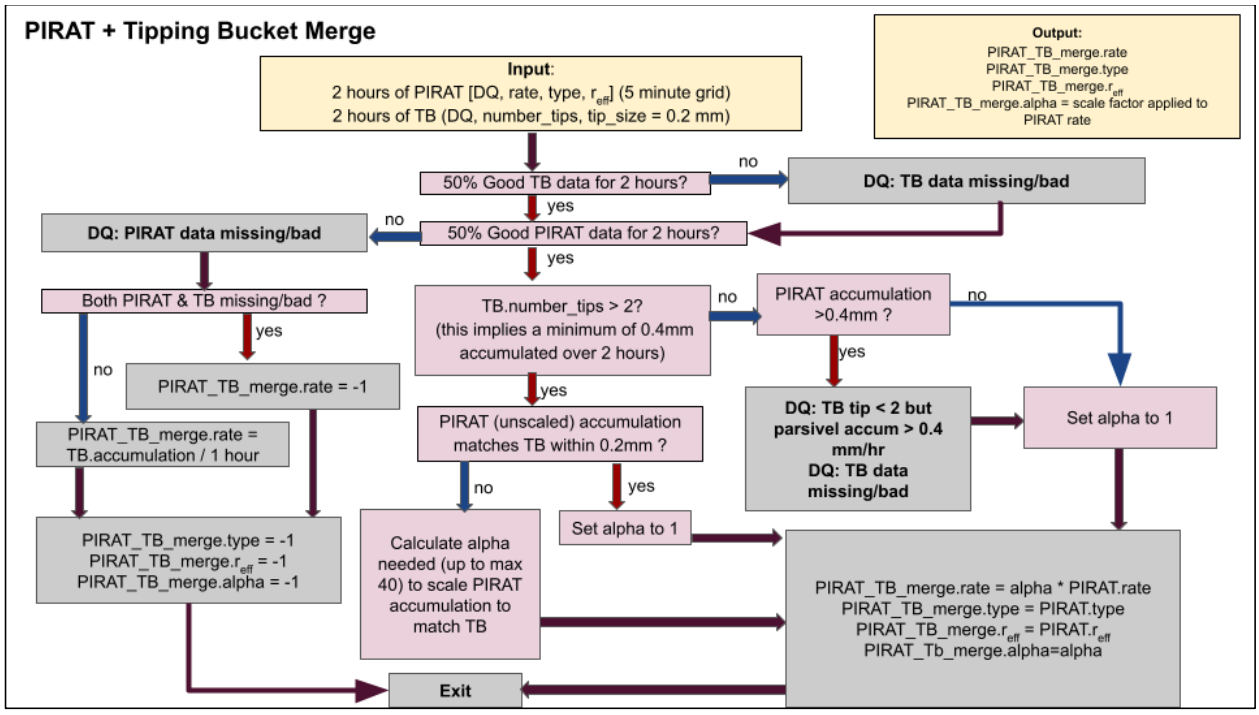

Figure S8: a) "PIRAT_TB_merge" subroutine flow chart. b) PDF comparison of 2-hour PIRAT and TB accumulations.

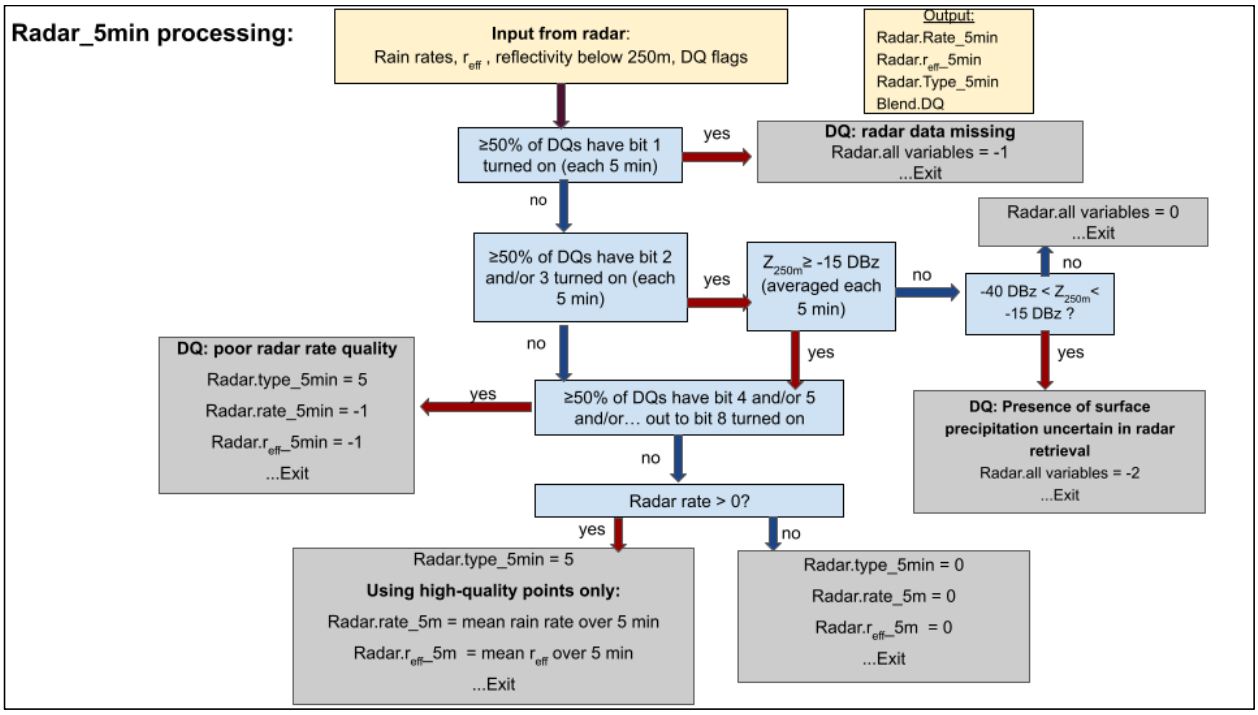

Figure S9: "Radar_xmin" subroutine flow chart.

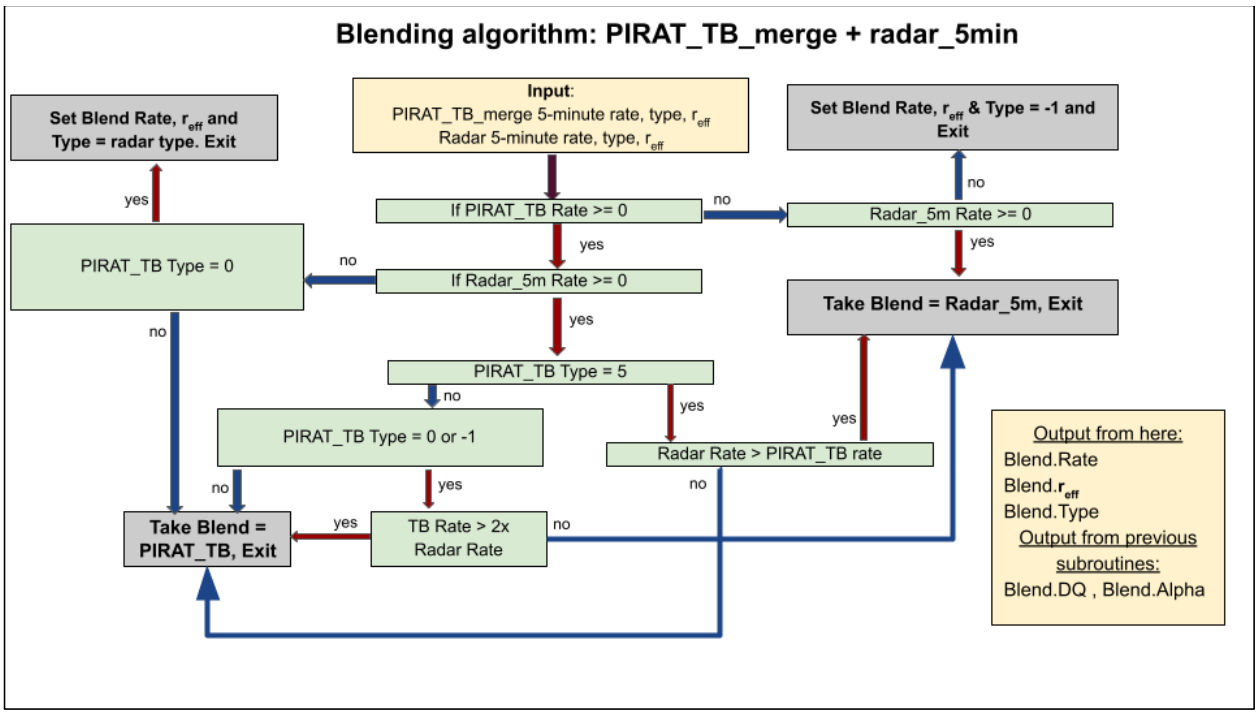

Figure S10: "Blend" subroutine flow chart.

485

(a)

Radar DQ flags

Bit 1: 'Bad, missing or questionable, radar data',
Bit 2: 'No lidar cloud base available (base set to 250 m)',
Bit 3: 'Lidar cloud base below 250 m',
Bit 4: 'Fall Velocity Estimate required extrapolating in Z (small dBZe out of range)',
Bit 5: 'Fall Velocity Estimate required extrapolating in Z (large dBZe out of range)',
Bit 6: 'Estimated Fall velocity less than 0.3 m/s (precipitation appears to be falling too slowly to be drizzle)',
Bit 7: 'Estimated Fall velocity exceed 3 m/s (falling too fast to be drizzle)',
Bit 8: 'Insufficient points to estimate Fall velocity.'

(b)

Blend DQ flags

Bit 0: PIRAT data missing/bad
Bit 1: TB data missing/bad
Bit 2: radar data missing
Bit 3: TB tip < 2 but parsivel accum > 0.4 mm/hr
Bit 4: poor radar rate quality
Bit 5: Presence of surface precipitation uncertain in radar retrieval

486

487 *Figure S11: data quality flags (a) of the radar ZV retrieval and (b) output by the blending*
488 *subroutines.*

489 **S3. Additional CloudSat Figures and Data**

490 In this appendix we examine CloudSat results by subdividing the data over a $10^o \times 10^o$ region into
491 three longitudinal bands (each $10^o \times 3.3^o$) to the west and east, as well as directly over the island,
492 and three latitudinal bands to the north and south of the island. Longitudinal variations for 2C-
493 Precip-Column, 2C-Snow-Profile and 2C-Rain-Profile are shown in Figs. S12-S14, respectively,
494 while latitudinal variations are shown in Figs. S15-S17. The variations in longitude are small
495 compared with those in latitude. 2C-Precip and 2C-Rain (Figs. S15 and S17, respectively) both
496 show large gradients in frequency of occurrence at all rain rates moving from south to north,
497 while 2C-Snow (Fig. S16) has a gradient in the opposite direction.

498 Tables S1-S3 list the 2C-Precip, 2C-Snow and 2C-Rain seasonal and annual mean precipitation
499 rates for 2006-2017 (in 2C-Snow's case, data was only available until 2016). Mean precipitation
500 rates are calculated in the same way as described in the main text (by including non-precipitating
501 periods where rate = 0 mm/hour, multiplied by the number of hours in each season). These
502 averages are for the center latitudinal band ($10^o \times 3.3^o$). The DJF column refers to December of
503 the year shown in the left column plus January and February of the next year (e.g. DJF 2016
504 means December 2016 plus January 2017 and February 2017), while other seasons the months
505 all come from the same year (e.g. MAM 2016 means March 2016, April 2016 and May 2016).
506 Table S4 gives the number of CloudSat overpasses in each season and annually from 2006-2017.

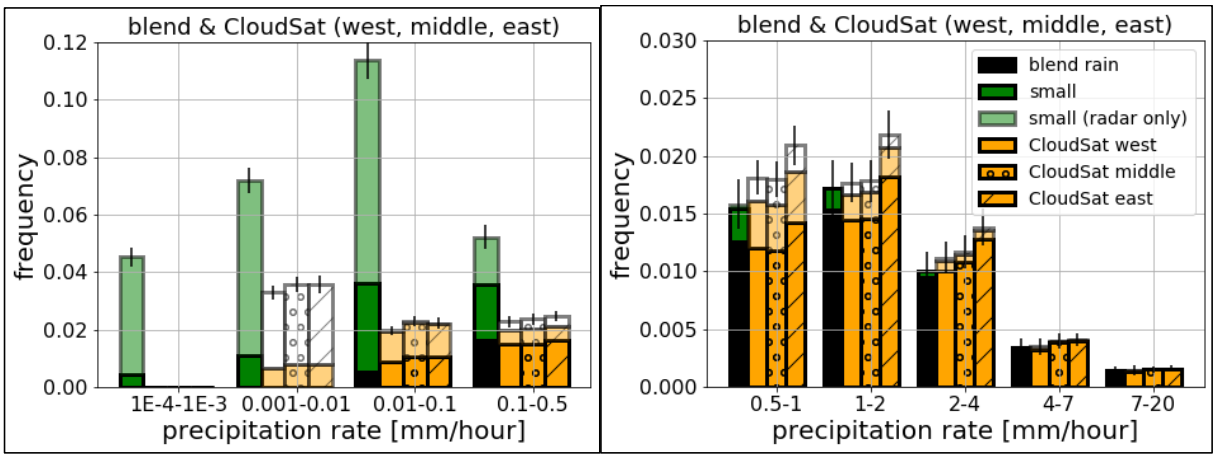

Figure S12: 2C-Precip-Column and blend rain rates for three longitudinal bands. Vertical axis is fraction of time that it rains at the rate specified. Black lines at the top of each colored bar show the estimated sampling uncertainty (defined as the standard deviation divided by the square root of overpasses for CloudSat and number of days for MICRE) as conservative estimate for the uncertainty in frequency of occurrence. Black bars = rain (large particles). Dark green = drizzle (small particles) seen by both radar and disdrometer. Light green = drizzle (small particles) seen by radar only. CloudSat bars are broken into three longitude bands (see legend). Dark orange bars = "rain certain". Light orange = "rain probable". White = "rain possible".

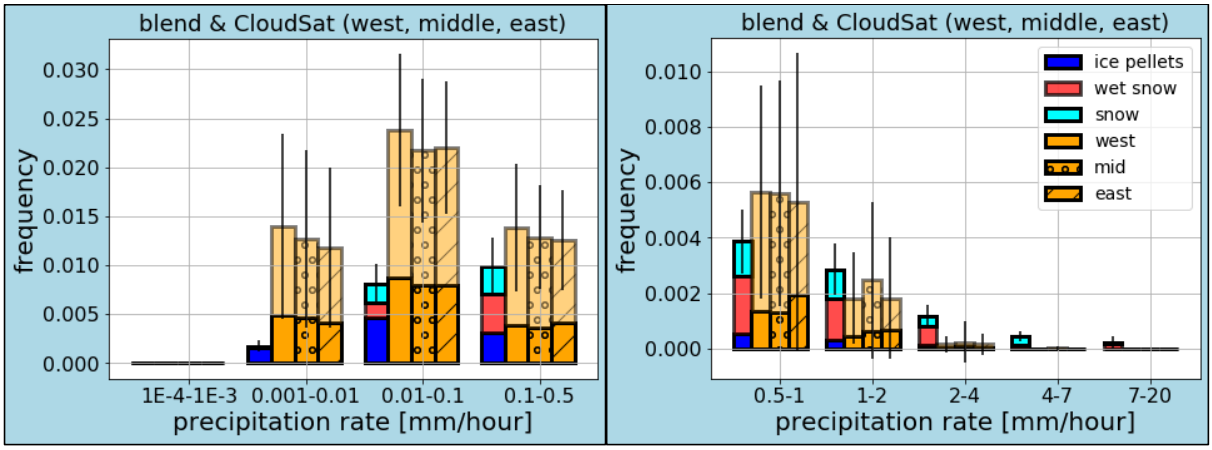

Figure S13: 2C-Snow-Profile and blend snowfall rates for three longitudinal bands. Vertical axis is fraction of time it snows at the rate specified. Error bars are the estimated sampling uncertainty. MICRE blend is divided into frozen types. CloudSat dark orange bars = "snow possible/certain." Light orange = "mixed possible/certain."

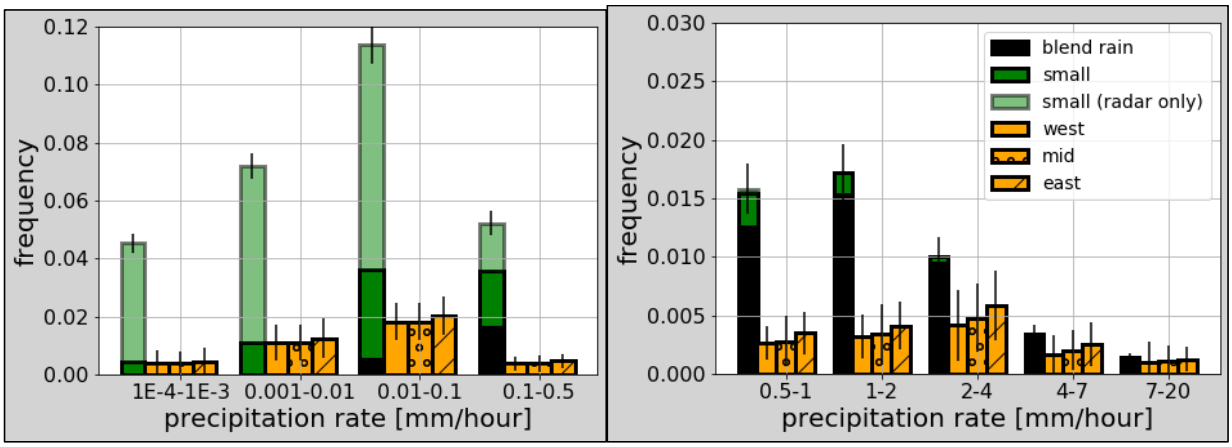

Figure S14: 2C-Rain-Profile and blend rain rates for three longitudinal bands. Vertical axis is fraction of time it rains at the rate specified. Error bars are the estimated sampling uncertainty. MICRE is the same as in Fig. S11. CloudSat dark orange bars = "rain certain."

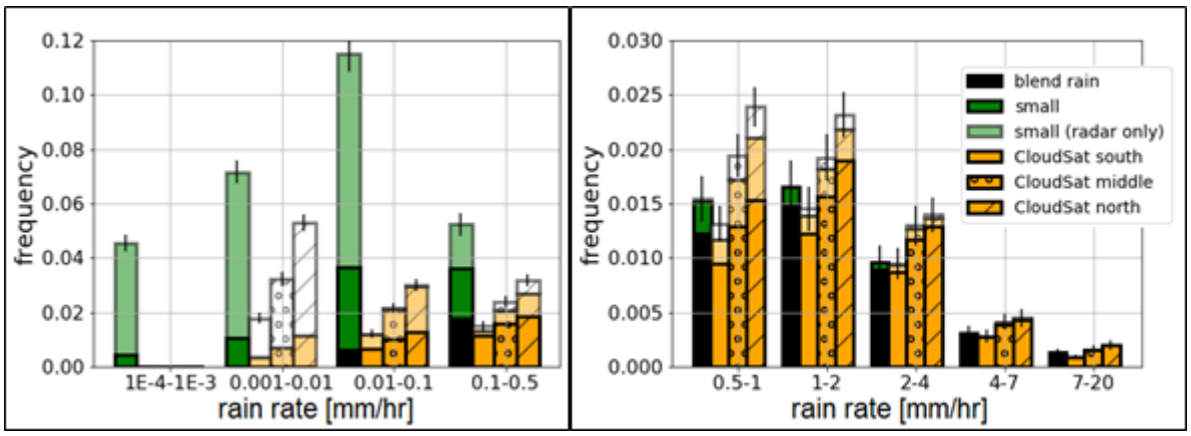

Figure S15: As in Fig. S12, but for latitudinal bands.

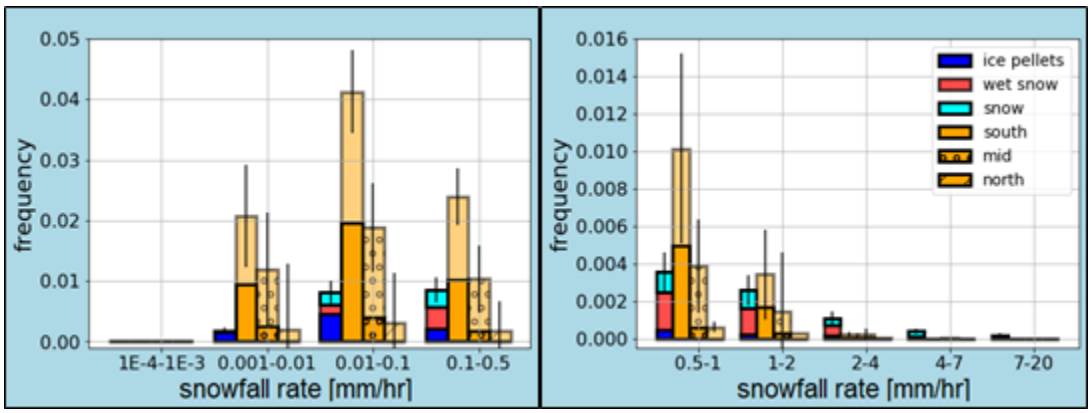

Figure S16: As in Fig. S13, but for latitudinal bands.

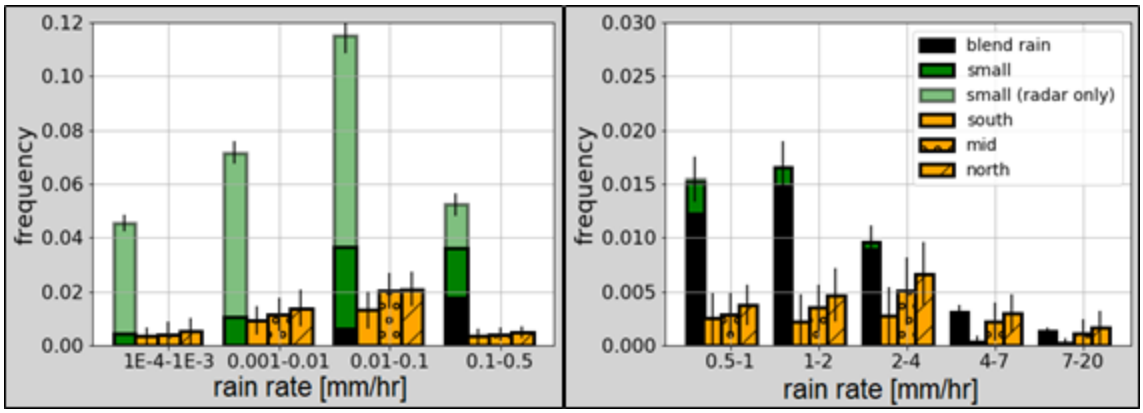

Figure S17: As in Fig. S14, but for latitudinal bands.

2C-Precip mean rain rates [mm/hour]	fall (MAM)	winter (JJA)	spring (SON)	summer (DJF)	annual
2006	NaN	0.330±0.157	0.103±0.047	0.093±0.027	NaN
2007	0.190±0.095	0.059±0.028	0.107±0.044	0.189±0.070	0.136±0.070
2008	0.160±0.038	0.130±0.058	0.122±0.058	0.302±0.100	0.179±0.064
2009	0.143±0.048	0.191±0.090	0.193±0.089	0.485±0.323	0.253±0.047
2010	0.248±0.089	0.073±0.024	0.279±0.101	0.218±0.070	0.205±0.071
2011	0.075±0.027	NaN	NaN	0.077±0.043	NaN
2012	0.222±0.098	0.049±0.022	0.030±0.019	0.470±0.178	0.193±0.079
2013	0.372±0.123	0.166±0.068	0.017±0.008	0.097±0.043	0.163±0.061
2014	0.137±0.051	0.138±0.108	0.030±0.013	0.136±0.077	0.110±0.062

2015	0.192±0.095	0.080±0.042	0.135±0.068	0.258±0.145	0.166±0.088
2016	0.206±0.086	0.157±0.093	0.159±0.071	0.179±0.049	0.175±0.075
2017	0.127±0.043	0.215±0.118	0.111±0.059	NaN	NaN
11-year average	0.188±0.072	0.144±0.073	0.117±0.052	0.228±0.102	0.169±0.075

532 *Table S1: 2C-Precip-Column seasonal and annual mean rain rates [mm/hr]. Annual means are*
533 *left out for years with incomplete datasets.*

2C-Snow mean rain rates [mm/hour]	fall (MAM)	winter (JJA)	spring (SON)	summer (DJF)	annual
2006	NaN	0.036±0.010	0.028±0.008	0	NaN
2007	0.015±0.009	0.028±0.006	0.017±0.005	0	0.019±0.006
2008	0.001±0.000	0.017±0.005	0.022±0.006	0.003±0.002	0.016±0.004
2009	0.003±0.002	0.019±0.006	0.017±0.004	0	0.014±0.004
2010	0.003±0.001	0.014±0.005	0.022±0.008	0	0.015±0.006
2011	0.002±0.002	NaN	NaN	0	NaN
2012	0.001±0.001	0.018±0.008	0.027±0.009	0	0.018±0.007
2013	0.002±0.001	0.034±0.015	0.032±0.013	0.001±0.001	0.025±0.010
2014	0.009±0.004	0.020±0.009	0.013±0.005	0	0.014±0.006

2015	0.007±0.006	0.061±0.023	0.025±0.007	0.012±0.009	0.030±0.011
2016	0.007±0.004	0.027±0.013	NaN	NaN	NaN
11-year average	0.005±0.003	0.027±0.010	0.023±0.007	0.002±0.001	0.014±0.005

Table S2: 2C-Snow-Profile annual accumulations [mm] broken into seasons. Data was available up until SON 2016 at the time of this project.

2C-Rain mean rain rates [mm/hour]	fall (MAM)	winter (JJA)	spring (SON)	summer (DJF)	annual
2006	NaN	0.205±0.126	0.009±0.005	0.039±0.017	NaN
2007	0.164±0.141	0.010±0.005	0.077±0.050	0.208±0.114	0.082±0.062
2008	0.089±0.035	0.061±0.037	0.044±0.035	0.109±0.043	0.060±0.036
2009	0.083±0.050	0.066±0.037	0.077±0.050	0.364±0.301	0.076±0.047
2010	0.129±0.088	0.015±0.009	0.143±0.076	0.106±0.047	0.108±0.062
2011	0.034±0.020	NaN	NaN	NaN	NaN
2012	NaN	0.006±0.004	0.007±0.006	0.143±0.083	0.005±0.004
2013	0.137±0.071	0.049±0.029	0.002±0.001	0.014±0.010	0.048±0.026
2014	0.028±0.017	0.053±0.050	0.001±0.001	0.053±0.043	0.021±0.017
2015	0.032±0.016	0.007±0.006	0.041±0.028	0.106±0.071	0.030±0.020
2016	0.111±0.094	0.085±0.064	0.040±0.027	0.042±0.015	0.069±0.053

2017	0.027±0.016	0.019±0.015	0.022±0.012	NaN	NaN
11-year average	0.080±0.050	0.052±0.035	0.042±0.041	0.212±0.172	0.096±0.071

Table S3: 2C-Rain-Profile seasonal and annual mean rain rates [mm/hr].

# CloudSat overpasses	fall (MAM)	winter (JJA)	spring (SON)	summer (DJF)	annual
2006	NAN	73	67	73	213
2007	65	75	73	68	281
2008	69	74	74	73	290
2009	72	77	79	44	272
2010	77	78	74	43	272
2011	35	NaN	6	23	64
2012	33	35	38	34	140
2013	37	40	37	37	151
2014	36	38	36	35	145
2015	35	39	38	39	151
2016	37	39	37	39	152
2017	40	17	35	3	95

Table S4: CloudSat overpasses (2006-2017). Highlighted overpass counts indicate too small of a sample size (resulting in NaN in tables S1-S3).

S4. Tipping bucket annual average precipitation rates by season

Average precipitation rates calculated using the tipping bucket timeseries from 2002 - 2017 are given in Table S5. Precipitation rates (measured in [mm/hour]) were calculated by dividing 3-hourly blocks of accumulated liquid [mm] by 3 hours. Uncertainty ranges in the table are the standard deviation divided by the square root of the number of 3 hour blocks. As in the CloudSat tables, the DJF row refers to December of the year shown on the left and the January + February of the subsequent year (e.g. DJF 2016 = December 2016, January and February 2017).

	fall (MAM)	winter (JJA)	spring (SON)	summer (DJF)	annual
2002	NaN	0.028±0.011	0.137±0.021	0.136±0.012	0.131±0.016
2003	0.140±0.022	0.104±0.011	0.079±0.012	0.102±0.012	0.100±0.013
2004	0.120±0.013	0.093±0.009	0.109±0.010	0.096±0.011	0.104±0.010
2005	0.150±0.012	0.143±0.012	0.107±0.015	0.157±0.015	0.140±0.013
2006	0.106±0.011	0.127±0.013	0.143±0.010	0.082±0.011	0.116±0.012
2007	0.142±0.016	0.070±0.008	0.115±0.020	0.129±0.017	0.117±0.013
2008	0.138±0.013	0.095±0.009	0.135±0.013	0.105±0.013	0.118±0.012
2009	0.110±0.010	0.086±0.009	0.080±0.014	0.129±0.015	0.100±0.011
2010	0.136±0.012	0.080±0.008	0.127±0.015	0.157±0.015	0.125±0.012
2011	0.121±0.012	0.121±0.019	0.139±0.010	0.095±0.009	0.119±0.018
2012	0.115±0.015	0.108±0.013	0.108±0.018	0.167±0.025	0.120±0.016

2013	0.165±0.015	0.123±0.014	0.102±0.013	0.132±0.013	0.131±0.012
2014	0.118±0.010	0.092±0.009	0.123±0.013	0.101±0.013	0.109±0.011
2015	0.143±0.014	0.130±0.012	0.113±0.014	0.139±0.015	0.130±0.013
2016	0.153±0.014	0.140±0.011	0.116±0.020	0.206±0.023	0.151±0.014
2017	0.082±0.012	0.177±0.026	NaN	NaN	NaN
15/16-year average	0.129±0.013	0.107±0.012	0.116±0.014	0.129±0.014	0.121±0.013

547 *Table S5: Tipping bucket average precipitation rates broken into years and seasons.*

S5. On the effect of CloudSat sampling in capturing annual and seasonal variability in accumulated surface precipitation

To examine the effect of sampling uncertainty on the ability of CloudSat to accurately measure annual and seasonal variability in accumulated surface precipitation, we sample from the tipping bucket record in a way that is consistent with CloudSat overpasses and compare accumulations based on the full tipping bucket with those based on this sampled version. Seasonal accumulations are obtained by determining the mean precipitation rate based on that season's samples and multiplying this mean rate by the duration of the season, and the annual accumulations are obtained by summing the seasonal components. In the plot below, we have generated correlation values for each season and annually based on true CloudSat overpass times, and 8 other versions (9 different colored points total) which represent the CloudSat sampling time shifted by 1 day each (from -4 to +4 days). That is, each "CloudSat sample" is simply the mean precipitation rate estimated from the tipping bucket over the 3 hour period which includes the CloudSat overpass.

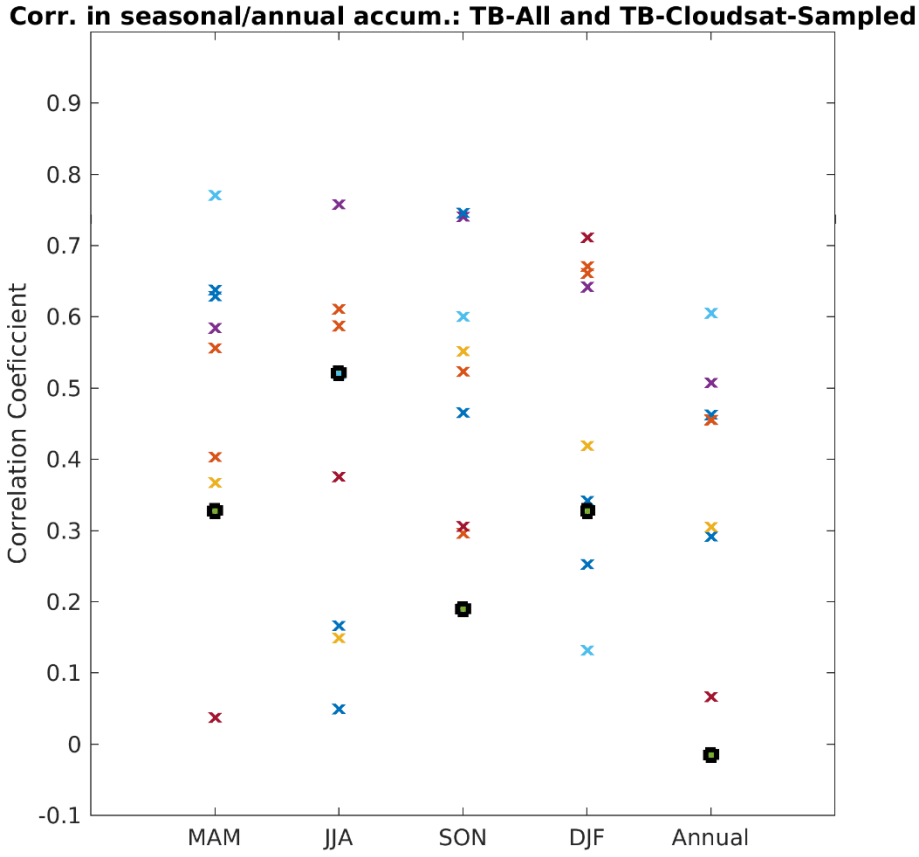

Figure S18: Correlation between accumulation in surface precipitation between the full Macquarie Island tipping bucket (TB) record and a sampled version of the TB record, sampled at actual CloudSat overpass times (black circles) and 8 other overpass schedules where the overpass time is shifted by 1 day each from -4 to +4 days (other colors).

As the figure shows, there is a large range in correlation values when comparing the full tipping bucket record to the various CloudSat-like sampled versions of the record. Some of the time the correlation is good, but sometimes the CloudSat-like sampled version happens to miss the large precipitation events, and sometimes it gets the large events and misses the dry periods. Perhaps humorously, the worst correlation (with a value slightly less than zero) occurs for the annual mean when using the actual timing of the CloudSat sampling; and indeed, the correlation between the actual CloudSat values and the tipping bucket is -0.1. And if CloudSat had launched one day later we might have obtained (again by chance) a seemingly high correlation value just over 0.6 in the annual mean.

Regardless, the important point here is that even for a "perfect retrieval," meaning one where CloudSat retrieved a precipitation rate for each overpass that perfectly matched the surface site, one will obtain a wide range of correlation coefficients because of the infrequent sampling. That is, precipitation events that occur on time scales faster than the sampling rate can and do contribute significantly to the accumulation. Consequently, CloudSat can NOT be used to meaningfully evaluate year-to-year variability in seasonal or annual accumulation because the sampling is too infrequent (even if the retrievals are of good quality).

S6. Comparison of Radar Doppler and Mean PIRAT Particle Velocities

As a simple evaluation of the PIRAT algorithm, we examine here the consistency between the radar observed Doppler velocities and PIRAT algorithm mean particle fall velocities. For the radar, we take 5-minute averages of the Doppler velocity at 116 m (the bin nearest to the surface with minimal clutter) and for the disdrometer, we calculate the average velocity from a 5-minute spectrum as:

$$v_{avg} = \frac{\sum_{i=1}^{32} \sum_{j=1}^{32} N_{i,j} \times v_j}{\sum_{i=1}^{32} \sum_{j=1}^{32} N_{i,j}}$$

where i is the size index, j is velocity index, $N_{i,j}$ is the number of particles in each size/velocity bin, v_j is the velocity for particles of size i, and v_{avg} is the mean particle fall velocity. For the example 5-minute spectrum shown below, the mean Parsivel particle fall velocity is 1.8 m/s.

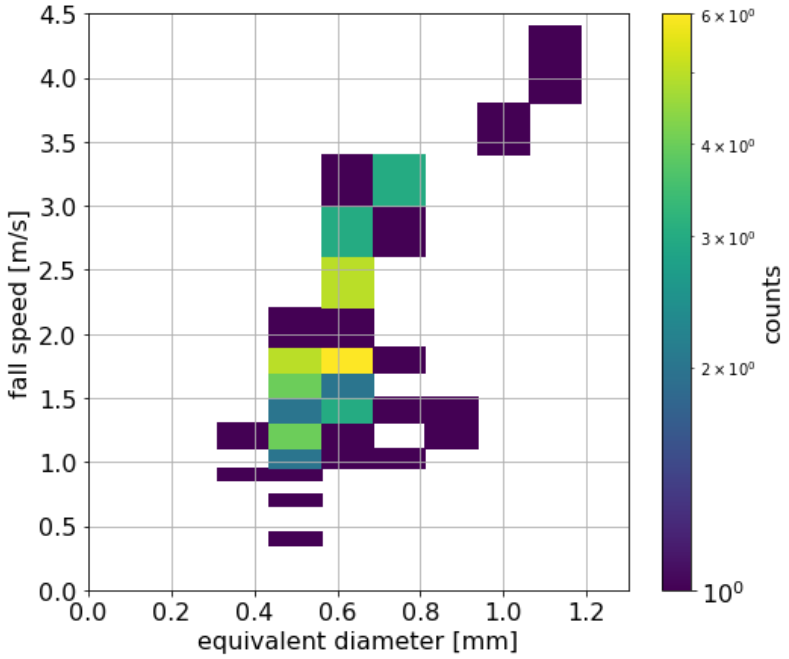

Figure S19: Sample corrected PIRAT particle size-velocity spectrum.

The two panels of Fig. S20 below show density-scatter plots of the radar Doppler and the Parsivel particle fall velocities for particles identified as rain or small. The left panel is from the PIRAT algorithm (including all corrections) and the right panel for the original raw spectra (uncorrected in any way). The left panel shows there is a strong correlation (pearson coefficient of 0.71) between the radar and PIRAT corrected velocities with a mode between 3 and 4 m/s (due to rain), while the uncorrected velocities in the right panels compare poorly with radar Doppler velocities. Below about 2 m/s the PIRAT algorithm fall velocities are slightly larger than those of the radar. These velocities are predominantly due to small particles. As discussed earlier, the Parsivel does not detect particles below ~0.5 mm well and so it is not surprising that the radar Doppler velocities (which will include contributions from all particles, including those too small to be detected by the Parsivel) might be somewhat lower (in spite of the fact that the radar mean Doppler velocities within individual radar range bins are reflectivity weighted). We note that in the blend product, rain rates and particle sizes for "small" precipitation are frequently based on the ZV retrieval which makes direct use of the radar Doppler velocity.

A similar comparison to that shown for rain and small particle types is given for snow, wet snow and ice (Figs. S21-23). For all three types of precipitation, the PIRAT algorithm reduces the scatter, suggesting the PIRAT corrections are having a positive effect. Most events identified as snow have a velocity between 1 and 2 m/s in both the radar and PIRAT, as one expects. Radar Doppler velocities larger than 3 m/s are likely snow misclassifications by PIRAT, and are relatively few in number. The comparison results for wet snow and ice are more difficult to interpret. For both types of precipitation the radar shows velocities typically between 1 to 4 m/s.

For wet snow, there is a clear maximum near 3 m/s in both the radar and PIRAT velocities, demonstrating some skill. Nonetheless, 28% of wet snow events have radar Doppler velocities between 1 and 2 m/s; if the particles are in fact mixed liquid-and-snow, they are either mostly snow or small in size. Somewhat similarly for ice pellets, there are a significant number (31%) of events where the PIRAT algorithm suggests a particle fall velocity between 2 and 3 m/s, but for which the radar Doppler data indicate a velocity below 2 m/s again, suggesting an ice pellet misclassification of a snow event or the presence of many smaller particles not measured by the Parsivel.

In some respects the disdrometer data and this analysis are ill-suited to the task of distinguishing between frozen/mixed precipitation phase classes. Additional analysis will eventually be undertaken with lidar depolarization data, pending processing of these data, which is ongoing.

PIRAT: Rain + Small

Raw Spectrum: Rain + Small

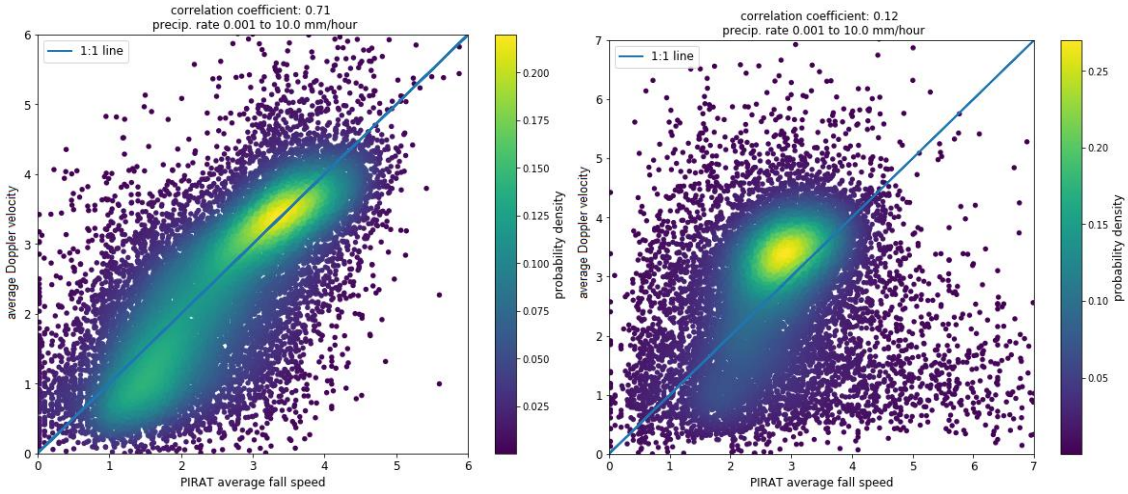

Figure S20: Density-scatter plot of the radar Doppler and Parsivel particle fall velocities for particles identified as rain or small with PIRAT corrections (left) and raw/uncorrected (right).

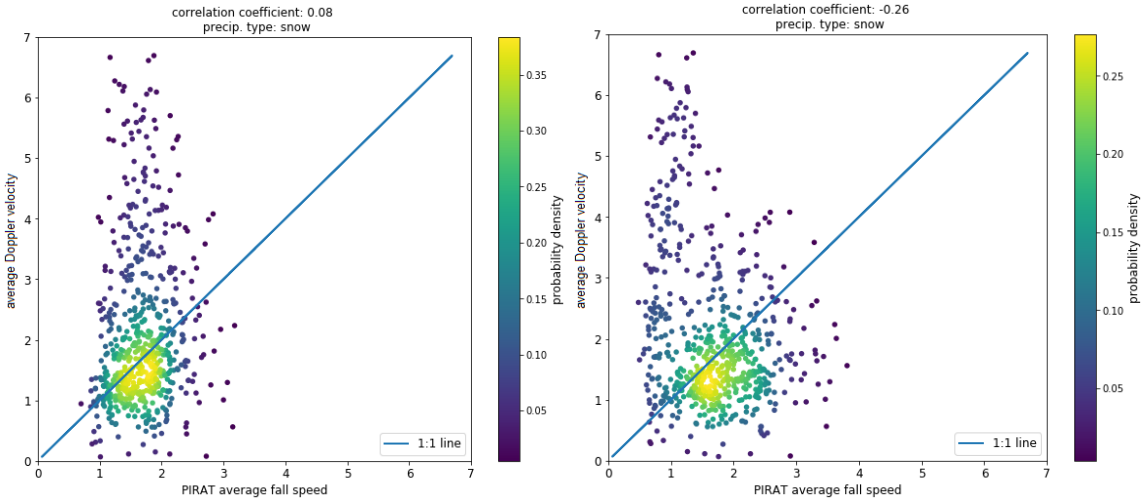

Figure S21: Same as Fig. S20, but for snow spectra.

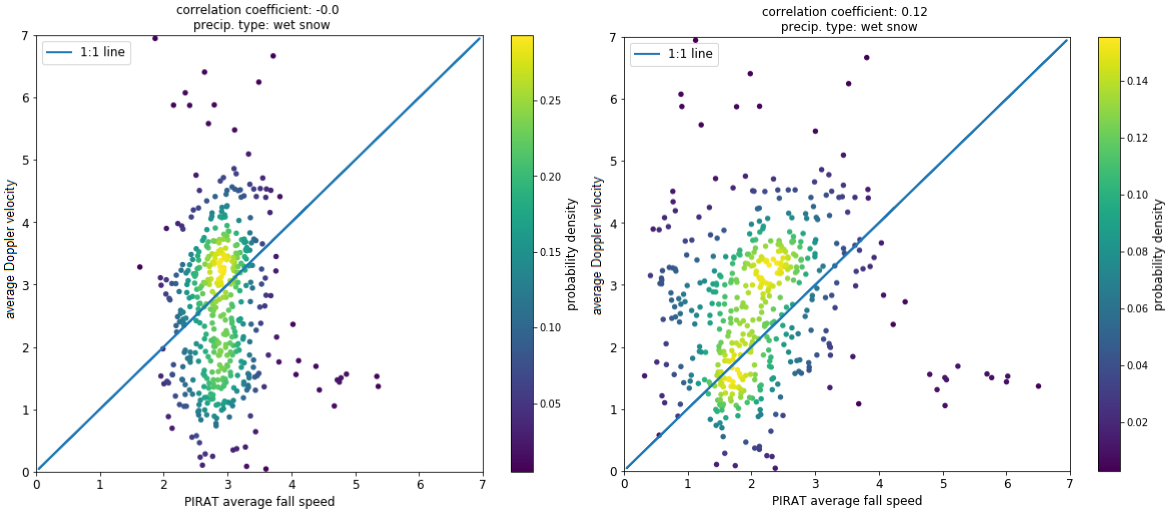

Figure S22: Same as Fig. S20, but for wet snow spectra.

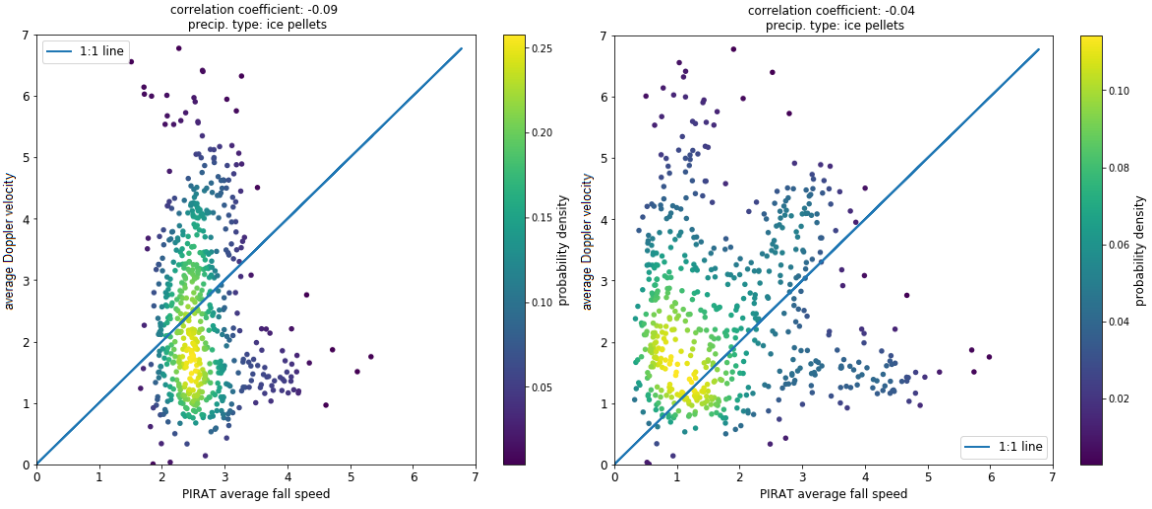

Figure S23: Same as Fig. S20, but for ice pellet spectra.

S6. Statistical significance of the diurnal cycle

Below are results from a bootstrap resampling hypothesis test. The null hypothesis is that the diurnal cycle is not significant. This is tested by resampling from the daily data with replacement and then aggregating the resampled data into 3-hour blocks to determine the difference in the precipitation taken at the hours of the maximum and minimum shown in the paper (Fig. 4a,b,c,d). The observed population of daily differences are resampled (10,000 times) to obtain a bootstrap estimate for the distribution of daily differences. The resampled (bootstrap) distributions are shown below for each category used in the paper. For instance, in Fig. S24, the bootstrap distribution is based on the difference in the frequencies of precipitation at 05:00 (03:30-06:30) LT minus 14:00 (12:30-15:30) LT observed each day. The 95% confidence interval around the resample distribution's mean diurnal range is then calculated. If the bounds of the confidence interval encompass zero, the diurnal range is not considered significant (there

is at least a 5% possibility that observed positive value for the diurnal difference could have happened "by chance"), and we cannot reject the null hypothesis. However, in all four plots the zero point is outside the lower tail, and so we do reject the hypothesis in all four cases, and conclude that there is (better than 95%) likely to be a diurnal cycle.

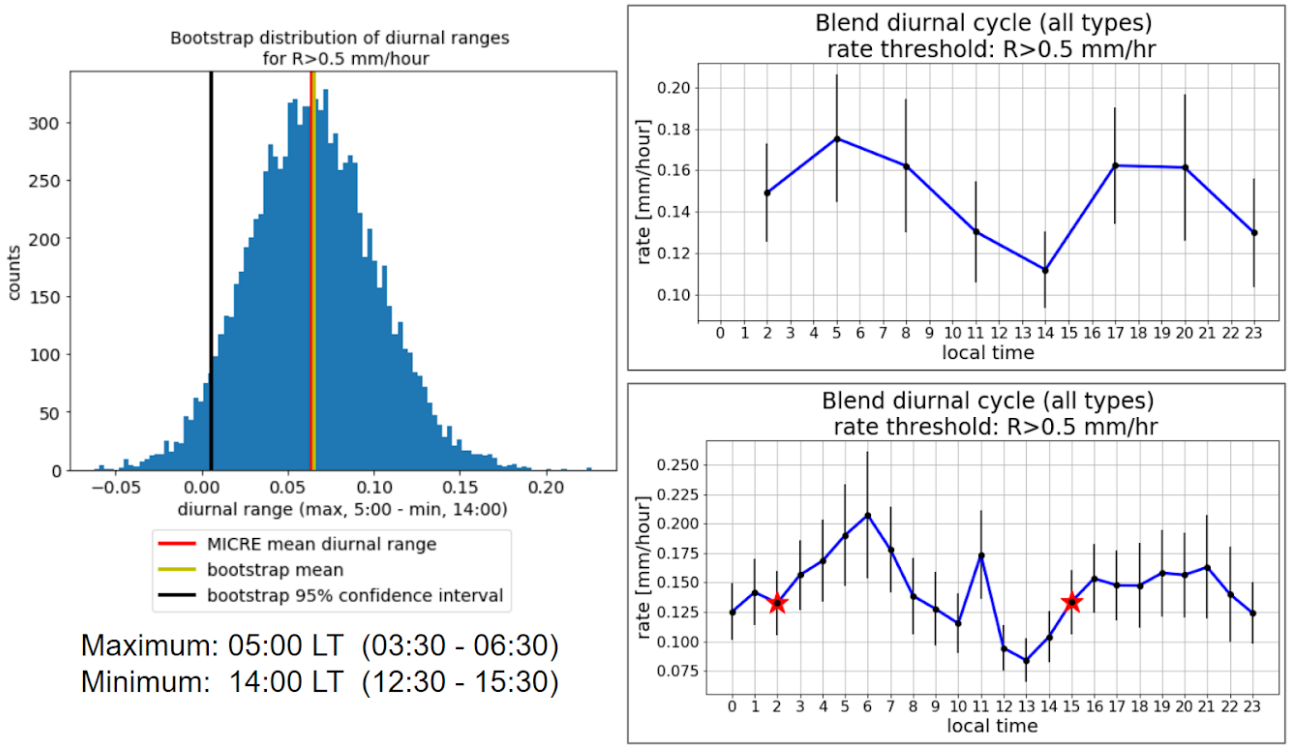

Fig. S24: Distribution of resamples (left) for the daily difference (max – min) precip. rate for moderate/heavy rates > 0.5 mm/hr, based on the 3-hourly data. Results for 1-hourly data are similar. The 24-hour diurnal cycle is shown in the right panels, aggregated into 3 hour blocks (top) and 1 hour blocks (bottom). The line shows mean values and error bars show uncertainty (standard deviation across days divided by the square root of the number of days). The resampled diurnal maximum & minimum for the significance testing are centered at 05:00 LT and 14:00 LT.

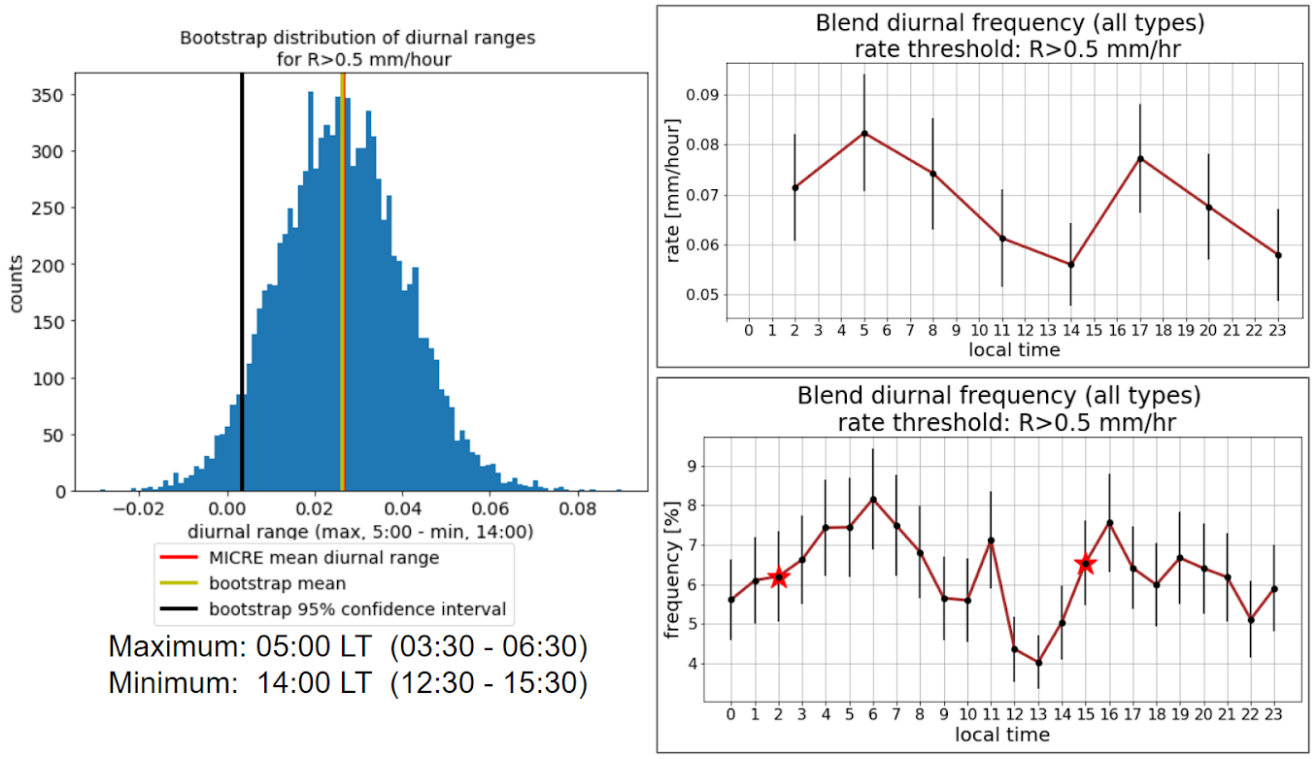

Fig. S25: Frequency-of-occurrence diurnal cycle for moderate/heavy rates (> 0.5 mm/hr).

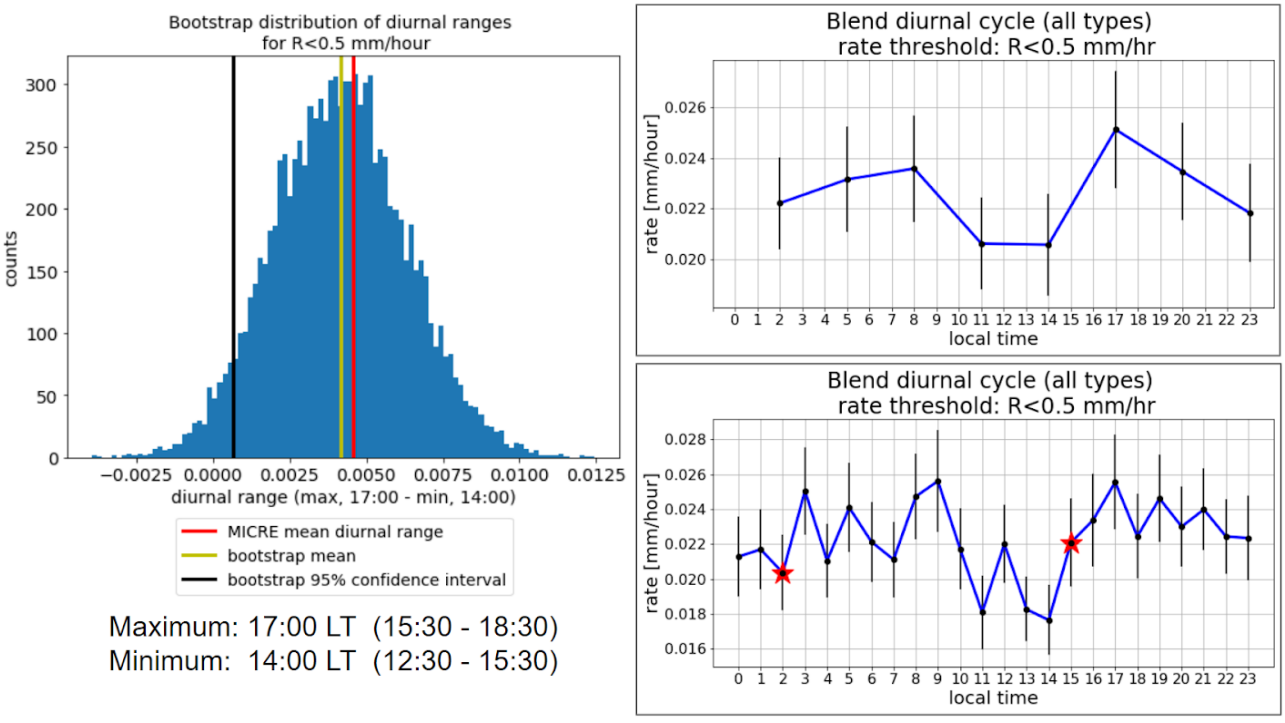

Fig. S26: Precip. rate diurnal cycle for light/moderate rates (< 0.5 mm/hr).

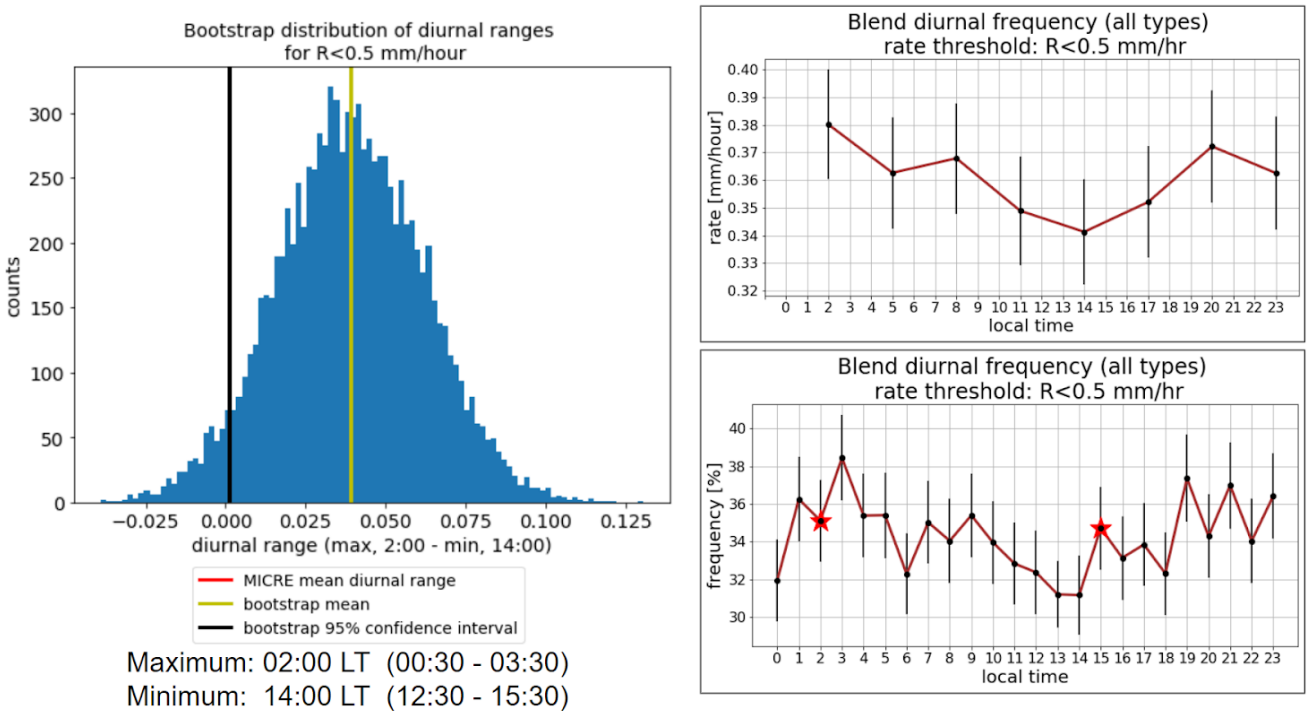

669

670 *Fig. S27: Frequency-of-occurrence diurnal cycle for light/moderate rates (< 0.5 mm/hr).*
671 *The resampled diurnal maximum & minimum for significance testing are centered at*
672 *02:00 LT and 14:00 LT.*